Inorganic Chemistry

Article

pubs.acs.org/IC

Influence of Lattice Interactions on the Jahn–Teller Distortion of the $[Cu(H_2O)_6]^{2+}$ Ion: Dependence of the Crystal Structure of $K_{2x}Rb_{2-2x}[Cu(H_2O)_6](SeO_4)_2$ upon the K/Rb Ratio

Charles J. Simmons,*[,†] Horst Stratemeier,[‡] Michael A. Hitchman,[‡] and Mark J. Riley[§]

[†]Division of Natural Sciences, University of Hawaii at Hilo, Hilo, Hawaii 96720-4091, United States

[‡]School of Chemistry, University of Tasmania, Box 252-75, Hobart, TAS 7001, Australia

[§]School of Chemistry and Molecular Biosciences, University of Queensland, St. Lucia, Queensland 4072, Australia

Supporting Information

ABSTRACT: The temperature dependence of the structures of a wide range of mixed-cation Tutton's salts of general formula $K_{2x}Rb_{2-2x}[Cu(H_2O)_6](SeO_4)_2$ has been determined over the temperature range 90 to 320 K. Crystals with a high proportion of potassium adopt a different structure (form **B**) from those with a low ratio (form **A**). In both forms, the $[Cu(H_2O)_6]^{2+}$ ion has an orthorhombically distorted tetragonally elongated coordination geometry, but the long and intermediate bonds occur with a different pair of water molecules in form **A** compared with form **B**. The alkali metal is surrounded by seven close oxygen atoms in form **B** but eight oxygen atoms in form **A**, and this difference in coordination number is associated with the change in the Cu–O bond distances via the hydrogen-bonding network. For crystals with between 32 and ~41% potassium, a relatively sharp change from form **B** to **A** occurs on cooling, and the temperature at which this occurs increases approximately linearly as the proportion of potassium falls. For the whole range of mixed crystals, the bond lengths have been determined as a function of temperature. The data have been interpreted as a thermal equilibrium of the two structural forms of the $[Cu(H_2O)_6]^{2+}$ ion that develops gradually as the temperature increases, with this becoming more pronounced as the proportions of the two cations become more similar. The temperature dependence of the bond lengths in this thermal equilibrium has been analyzed using a model in which the Jahn–Teller potential surface of the $[Cu(H_2O)_6]^{2+}$ ion is perturbed by lattice strain interactions. The magnitude and sign of the orthorhombic component of this strain interaction depends upon the proportion of potassium to rubidium ions in the structure.

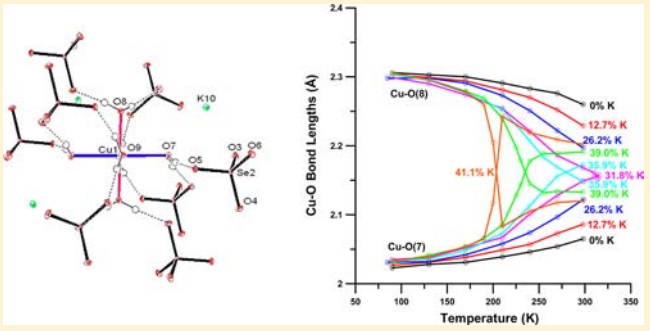

INTRODUCTION

The copper(II) Tutton's salts[1] of general formula $X_2[Cu(H_2O)_6](YO_4)_2$, where X represents a monovalent cation and Y is either S or Se, provide good examples of the way in which the interplay of Jahn–Teller (JT) vibronic coupling and lattice forces decide the structure adopted by the $[Cu(H_2O)_6]^{2+}$ ion. The ammonium copper(II) sulfate Tutton's salt is especially interesting because it exists in two distinct forms. When deuterated, it adopts a structure (form **A**) in which the long axis of the distorted $[Cu(D_2O)_6]^{2+}$ ion occurs to the pair of O(8) water molecules,[2] whereas in the hydrogenous salt (form **B**), this direction is to the O(7) waters.[3] This change is accompanied by slight alterations in the orientations and hydrogen-bonding interactions involving the ammonium and sulfate groups.[4] The deuterated compound may be switched to form **B** by irradiation in the infrared region[5] or doping with a trace of Zn^{2+}.[6] Application of pressure also causes the deuterated compound to switch to form **B**,[4,7] with this change exhibiting hysteresis when the pressure is decreased.[8,9] If the compound is cooled before the pressure is released, it remains in form **B**.[10] Both $(NH_4)_2[Cu(H_2O)_6](SO_4)_2$ and its deuterated analogue exhibit changes in the observed Cu–O bond lengths as a function of temperature.[2,11] Interestingly, the analogous chromium hydrogenous and deuterated salts both adopt form **A**,[12] though the deuterated compound switches to form **B** under pressure,[13] and the hydrogenous compound also switches to form **B** upon doping with trace amounts of Zn^{2+}.[14]

Of particular interest is the cause of the structural change in the copper(II) compound upon deuteration. A highly accurate neutron diffraction study of $(ND_4)_2[Cu(D_2O)_6](SO_4)_2$ prepared in the pressure-induced metastable state of crystal modification **B** found that the bond lengths and hydrogen-bond distances are very similar to those in the corresponding hydrogenous salt.[10] This implies that there is a very delicate balance between the two modifications, with the structural switch being associated with subtle differences in the hydrogen-bonding interactions, either involving the copper(II) complex

Received: May 31, 2013
Published: September 6, 2013

   dx.doi.org/10.1021/ic401385f | Inorg. Chem. 2013, 52, 10481–10499

or throughout the lattice as a whole.[4,5,10] A second point of interest concerns the thermal equilibria. Unlike most other copper(II) compounds exhibiting such behavior,[15] the proportions of the two forms differ significantly from a simple averaging of their thermal population at higher temperatures.[11] In the original neutron diffraction analysis of the deuterated compound, the thermal equilibrium was ascribed to the development of rotational motion of the ammonium group,[2] and this explanation has been developed in a more recent study.[16] In this context, it has been found that optical pumping of a vibrational mode associated with this rotational motion causes a structural switch for the partially deuterated compound.[5] Alternatively, it has been proposed that the anomalous thermal behavior may be caused by cooperative interactions between the neighboring $[Cu(D_2O)_6]^{2+}$ complexes in the crystal lattice.[11]

To provide further information on these questions, a series of crystals with varying proportions of deuterium was studied by electron paramagnetic resonance (EPR) spectroscopy.[17] It was found that the structural switch occurs quite sharply at ∼50% deuterium, with the thermal equilibrium of the compound with 42% deuterium being similar to that of the pure hydrogenous compound. This suggests that the study of other mixed crystals might be fruitful. As far as the disposition of the Cu−O bond lengths is concerned, the compounds $K_2[Cu(H_2O)_6](SO_4)_2$, $Rb_2[Cu(H_2O)_6](SO_4)_2$, and $Rb_2[Cu(H_2O)_6](SeO_4)_2$ all adopt form **A**.[7,18] The compound $K_2[Cu(H_2O)_6](SeO_4)_2$, however, exists in the form **B** crystal modification.[19] Therefore, replacement of SO_4^{2-} with SeO_4^{2-} in the potassium compound, or the replacement of Rb^+ with K^+ in the selenate compound, results in a switch from form **A** to form **B**. Data for the mixed-crystal series $K_2[Cu(H_2O)_6](SO_4)_{2-2x}(SeO_4)_{2x}$ was reported recently,[20] and the structure was found to change from form **B** to form **A** as the proportion of sulfate increased from 25 to 68%. A thermal equilibrium between the forms was observed for all the mixed compositions of $K_2[Cu(H_2O)_6](SO_4)_{2-2x}(SeO_4)_{2x}$, with the temperature dependence becoming more pronounced as the proportion of SO_4^{2-} approached that of SeO_4^{2-}. Although subsequent attempts to prepare mixed crystals with $(SO_4^{2-})/(SeO_4^{2-})$ ratios between these limits were successful, the quality of the X-ray data was marginal due to poor crystal quality, so it was impossible to investigate the composition region where the structural switch is expected to be most delicately balanced.[21]

The present paper describes the results of a similar study of the series $K_{2x}Rb_{2-2x}[Cu(H_2O)_6](SeO_4)_2$. The cause of the structural switch, and the nature of any thermal equilibrium, should be simpler to understand in these compounds, as, unlike the ammonium group, the alkali metal cations do not participate in hydrogen-bonding interactions. In this case, mixed crystals covering most of the composition range have been obtained, allowing the influence of the cation on the structural switch to be studied in considerable detail.

EXPERIMENTAL SECTION

Preparation of Compounds. *$K_2[Cu(H_2O)_6](SeO_4)_2$.* An aqueous solution (30 mL) of 2.21 g (0.01 mol) of K_2SeO_4 (Aldrich) was added to an aqueous solution (30 mL) of 2.96 g (0.01 mol) of $CuSeO_4·5H_2O$ (Alfa Aesar); the resulting mixture was made slightly acidic by the dropwise addition of H_2SeO_4 and then allowed to evaporate slowly until near dryness. $Rb_2[Cu(H_2O)_6](SeO_4)_2$: 2.3 g (0.01 mol) of Rb_2CO_3 (Aldrich) was suspended in 5 mL of water, and enough H_2SeO_4 was slowly added until all the carbonate dissolved. This solution was then added to an aqueous solution (20 mL) of 2.96 g (0.01 mol) of $CuSeO_4·5H_2O$ (Alfa Aesar), and the resulting mixture was allowed to evaporate to near dryness. Crystals involving mixed cations were grown by recrystallizing mixtures of the pure salts with appropriate molar ratios of potassium to rubidium in deionized water.

X-Ray Crystal Structure Determinations. Single crystals from each batch were ground to spheres of approximate radius 0.30 mm and mounted on the tips of glass fibers with quick-drying epoxy glue. X-ray diffraction data were first collected at room temperature using graphite monochromated Mo Kα radiation (λ = 0.71069 Å) on a Nonius Kappa CCD diffractometer equipped with an Oxford Model 700 Cryostream cooler. Each data set was measured using a combination of φ and ω scans with κ offsets. The data frames were integrated and scaled using the *HKL* suite of *XdisplayF*, *Denzo*, and *Scalepack*.[22] Unit cell parameters were retrieved and refined on all reflections.

The ratio of K^+ to Rb^+ for mixed crystals for which the concentration of K^+ was greater than that of Rb^+ was determined by using the known positional parameters for the non-hydrogen atoms of pure $K_2[Cu(H_2O)_6](SeO_4)_2$[19,20] and those of Rb^+ from pure $Rb_2[Cu(H_2O)_6](SeO_4)_2$[18] as starting parameters for the refinement of each structure. Conversely, if the concentration of K^+ was less than that of Rb^+, then the positional parameters for the non-hydrogen atoms of pure $Rb_2[Cu(H_2O)_6](SeO_4)_2$ and those for K^+ from pure $K_2[Cu(H_2O)_6](SeO_4)_2$ were used as starting coordinates. An initial value for the parameter describing the K^+/Rb^+ ratio used in the refinements was based on the molar ratio of K^+/Rb^+ used in the chemical syntheses. This initial model was refined anisotropically (K^+ and Rb^+ isotropically), and the hydrogen atoms were located in a Fourier difference map. To check the validity of the occupancy parameters $x(K^+)$ and $x(Rb^+)$, they were first allowed to vary unconstrained, and it was found that their sum converged to 1.00 ± 0.01. In some structures their values were arbitrarily increased or decreased, but in every case they returned to the same values. In the final least-squares analysis for each structure, all non-H atoms were refined with anisotropic displacement parameters and H atoms with isotropic displacement parameters, and the sum of the occupancies of K^+ and Rb^+ was constrained to be equal to 1.0. In this way, the ratios of K^+/Rb^+ were determined to within ∼1%.[23] A plot of unit cell volume at ambient temperature vs percent K^+ dopant shows only a slight deviation from Vegard's law (Figure 1). All crystallographic calculations were performed using Molecular Structure Corporation's *teXsan* for Windows v. 1.06.[24]

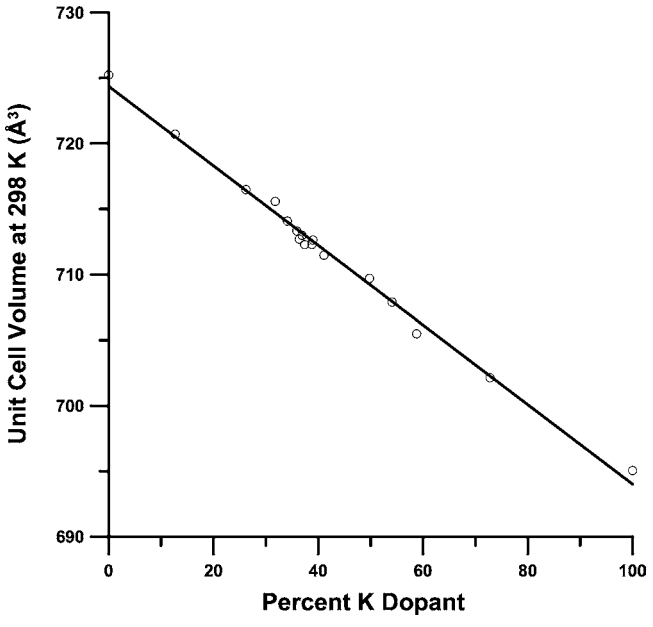

Figure 1. Plot of unit cell volume for mixed $K_{2x}Rb_{2-2x}[Cu(H_2O)_6](SeO_4)_2$ crystals as a function of percent K^+ dopant at 298 K.

dx.doi.org/10.1021/ic401385f | *Inorg. Chem.* 2013, 52, 10481−10499

Table 1. M−O Bond Lengths (Å) and Differences in Mean-Square Displacement Amplitudes along M−O Bond Directions ΔU_{obs}[(M−O)] (Å^2), M = Cu and Zn

T (K)	Cu−O(7)	Cu−O(8)	Cu−O(9)	ΔU_{obs}[Cu−O(7)]	ΔU_{obs}[Cu−O(8)]	ΔU_{obs}[Cu−O(9)]
			$Rb_2[Cu(H_2O)_6](SeO_4)_2$, x = 0.000			
90	2.023(1)	2.306(1)	1.947(2)	0.0034(5)	0.0038(6)	0.0021(5)
130	2.028(1)	2.303(2)	1.946(1)	0.0035(5)	0.0046(6)	0.0023(5)
170	2.031(2)	2.300(2)	1.944(2)	0.0047(8)	0.0037(8)	0.0012(8)
210	2.039(1)	2.291(2)	1.945(2)	0.0054(7)	0.0077(7)	0.0028(6)
240	2.046(2)	2.283(2)	1.945(2)	0.0072(8)	0.0093(9)	0.0029(8)
270	2.054(2)	2.276(2)	1.947(2)	0.0086(8)	0.0100(8)	0.0023(7)
298	2.065(2)	2.260(2)	1.944(2)	0.0088(8)	0.0137(8)	0.0020(7)
			$K_{2x}Rb_{2-2x}[Cu(H_2O)_6](SeO_4)_2$, x = 0.127			
90	2.027(1)	2.303(1)	1.946(1)	0.0043(5)	0.0025(5)	0.0023(5)
130	2.031(2)	2.299(2)	1.945(2)	0.0039(5)	0.0050(5)	0.0019(5)
170	2.038(1)	2.294(1)	1.945(1)	0.0051(5)	0.0045(6)	0.0022(5)
210	2.049(2)	2.281(2)	1.945(2)	0.0081(9)	0.0091(9)	0.0016(8)
240	2.057(2)	2.270(3)	1.947(2)	0.0113(9)	0.0120(4)	0.0012(8)
270	2.073(1)	2.252(1)	1.946(1)	0.0114(5)	0.0138(5)	0.0029(4)
298	2.086(3)	2.229(3)	1.944(2)	0.0179(12)	0.0150(11)	0.0008(10)
			$K_{2x}Rb_{2-2x}[Cu(H_2O)_6](SeO_4)_2$, x = 0.262			
85	2.031(1)	2.298(1)	1.946(1)	0.0041(5)	0.0050(5)	0.0012(5)
130	2.032(1)	2.298(1)	1.944(1)	0.0042(5)	0.0050(5)	0.0022(5)
170	2.042(1)	2.291(1)	1.943(1)	0.0050(6)	0.0068(6)	0.0016(5)
210	2.058(1)	2.273(1)	1.946(1)	0.0075(4)	0.0096(5)	0.0024(4)
240	2.074(1)	2.251(1)	1.944(1)	0.0101(6)	0.0151(6)	0.0020(5)
270	2.097(1)	2.222(2)	1.944(1)	0.0144(6)	0.0170(7)	0.0030(5)
298	2.122(2)	2.197(2)	1.946(2)	0.0180(7)	0.0192(7)	0.0020(5)
			$K_{2x}Rb_{2-2x}[Cu(H_2O)_6](SeO_4)_2$, x = 0.318			
90	2.035(1)	2.299(1)	1.944(1)	0.0046(3)	0.0044(3)	0.0033(3)
130	2.038(1)	2.290(2)	1.940(1)	0.0050(5)	0.0066(6)	0.0023(5)
170	2.052(1)	2.274(1)	1.940(1)	0.0087(5)	0.0089(6)	0.0032(5)
210	2.067(1)	2.254(1)	1.939(1)	0.0124(5)	0.0157(6)	0.0036(4)
240	2.101(1)	2.221(1)	1.940(1)	0.0148(4)	0.0177(5)	0.0024(4)
270	2.128(2)	2.186(2)	1.939(1)	0.0191(7)	0.0191(7)	0.0034(6)
298	2.149(1)	2.168(1)	1.941(1)	0.0194(5)	0.0212(5)	0.0017(4)
310	2.154(2)	2.161(2)	1.944(2)	0.0227(9)	0.0208(9)	0.0053(8)
315	2.158(2)	2.153(2)	1.940(2)	0.0212(11)	0.0216(10)	0.0030(9)
			$K_{2x}Rb_{2-2x}[Cu(H_2O)_6](SeO_4)_2$, x = 0.359			
90	2.032(1)	2.303(1)	1.944(1)	0.0046(4)	0.0036(4)	0.0029(4)
130	2.036(1)	2.295(1)	1.943(1)	0.0064(5)	0.0053(5)	0.0026(5)
170	2.048(1)	2.277(1)	1.942(1)	0.0078(5)	0.0092(6)	0.0019(5)
210	2.073(2)	2.253(2)	1.942(2)	0.0112(7)	0.0128(7)	0.0041(6)
240	2.113(2)	2.207(2)	1.941(1)	0.0166(5)	0.0202(5)	0.0034(4)
255	2.135(2)	2.183(2)	1.936(2)	0.0196(7)	0.0187(7)	0.0030(6)
270	2.156(2)	2.169(2)	1.940(1)	0.0188(5)	0.0201(4)	0.0030(3)
298	2.172(2)	2.148(2)	1.943(1)	0.0223(8)	0.0206(7)	0.0028(6)
			$K_{2x}Rb_{2-2x}[Cu(H_2O)_6](SeO_4)_2$, x = 0.390			
90	2.0313(9)	2.305(1)	1.9451(9)	0.0037(3)	0.0034(3)	0.0028(3)
130	2.041(1)	2.296(1)	1.941(1)	0.0047(5)	0.0063(5)	0.0022(5)
170	2.053(1)	2.279(2)	1.942(1)	0.0070(5)	0.0082(6)	0.0019(5)
190	2.066(1)	2.269(1)	1.942(1)	0.0096(5)	0.0108(5)	0.0025(4)
210	2.085(2)	2.240(2)	1.942(1)	0.0137(6)	0.0149(6)	0.0035(5)
225	2.128(2)	2.198(2)	1.942(2)	0.0194(8)	0.0188(8)	0.0028(7)
230	2.143(2)	2.179(2)	1.943(2)	0.0187(9)	0.0188(8)	0.0013(7)
235	2.162(3)	2.162(2)	1.943(2)	0.0211(10)	0.0196(9)	0.0018(8)
240	2.178(2)	2.145(2)	1.946(1)	0.0196(6)	0.0191(6)	0.0008(5)
255	2.189(2)	2.132(2)	1.942(1)	0.0190(8)	0.0161(8)	0.0013(6)
270	2.189(2)	2.134(2)	1.943(1)	0.0191(7)	0.0179(6)	0.0021(5)
298	2.191(1)	2.133(1)	1.943(1)	0.0192(6)	0.0185(5)	0.0031(4)
			$K_{2x}Rb_{2-2x}[Cu(H_2O)_6](SeO_4)_2$, x = 0.411			
90	2.033(1)	2.304(1)	1.941(1)	0.0033(4)	0.0047(4)	0.0028(4)
130	2.039(1)	2.296(1)	1.941(1)	0.0057(5)	0.0059(5)	0.0023(5)
170	2.054(1)	2.278(1)	1.943(1)	0.0081(4)	0.0089(4)	0.0030(4)

dx.doi.org/10.1021/ic401385f | Inorg. Chem. 2013, 52, 10481−10499

Table 1. continued

T (K)	Cu−O(7)	Cu−O(8)	Cu−O(9)	ΔU_{obs}[Cu−O(7)]	ΔU_{obs}[Cu−O(8)]	ΔU_{obs}[Cu−O(9)]
			$K_{2x}Rb_{2-2x}[Cu(H_2O)_6](SeO_4)_2$, x = 0.411			
190	2.070(1)	2.259(1)	1.940(1)	0.0096(5)	0.0142(5)	0.0032(4)
200	2.117(3)	2.204(3)	1.937(5)	0.0179(11)	0.0198(11)	0.0026(10)
210	2.243(2)	2.083(2)	1.940(2)	0.0117(7)	0.0131(7)	0.0026(6)
240	2.219(2)	2.105(2)	1.942(2)	0.0165(5)	0.0158(5)	0.0012(5)
270	2.209(1)	2.118(1)	1.943(1)	0.0164(6)	0.0177(6)	0.0016(5)
298	2.202(2)	2.120(2)	1.944(1)	0.0193(7)	0.0177(6)	0.0023(5)
			$K_{2x}Rb_{2-2x}[Cu(H_2O)_6](SeO_4)_2$, x = 0.498			
90	2.295(1)	2.036(1)	1.945(1)	0.0033(4)	0.0040(4)	0.0025(4)
130	2.289(1)	2.043(1)	1.944(1)	0.0045(5)	0.0043(5)	0.0016(5)
170	2.278(1)	2.052(1)	1.945(1)	0.0068(5)	0.0059(5)	0.0019(5)
210	2.266(1)	2.063(1)	1.941(1)	0.0100(5)	0.0087(5)	0.0028(4)
240	2.250(1)	2.077(1)	1.941(1)	0.0124(5)	0.0107(5)	0.0020(4)
270	2.239(2)	2.088(1)	1.941(1)	0.0141(6)	0.0133(6)	0.0021(5)
298	2.226(1)	2.098(1)	1.941(1)	0.0161(6)	0.0151(5)	0.0022(4)
			$K_{2x}Rb_{2-2x}[Cu(H_2O)_6](SeO_4)_2$, x = 0.728			
90	2.305(1)	2.034(1)	1.943(1)	0.0027(4)	0.0025(4)	0.0021(4)
140	2.3016(8)	2.0365(8)	1.9425(8)	0.0041(3)	0.0034(3)	0.0024(3)
190	2.2929(9)	2.0433(9)	1.9442(8)	0.0053(3)	0.0054(3)	0.0025(3)
220	2.288(1)	2.050(1)	1.940(1)	0.0061(4)	0.0070(4)	0.0023(4)
250	2.282(1)	2.057(1)	1.940(1)	0.0072(4)	0.0081(4)	0.0023(4)
298	2.268(1)	2.066(1)	1.941(1)	0.0111(5)	0.0110(4)	0.0026(4)
			$K_2[Cu(H_2O)_6](SeO_4)_2$, x = 1.000			
85	2.3161(8)	2.0326(8)	1.9420(8)	0.0020(3)	0.0024(3)	0.0023(3)
170	2.3125(9)	2.0350(9)	1.9402(8)	0.0030(3)	0.0031(3)	0.0029(3)
210	2.306(1)	2.035(1)	1.941(1)	0.0038(5)	0.0042(4)	0.0020(4)
240	2.302(1)	2.039(1)	1.940(1)	0.0064(6)	0.0050(5)	0.0021(5)
298	2.297(1)	2.050(1)	1.941(1)	0.0077(5)	0.0079(4)	0.0036(4)
320	2.293(2)	2.052(1)	1.940(2)	0.0087(7)	0.0075(6)	0.0036(6)
T (K)	Zn−O(7)	Zn−O(8)	Zn−O(9)	ΔU_{obs}[Zn−O(7)]	ΔU_{obs}[Zn−O(8)]	ΔU_{obs}[Zn−O(9)]
			$Rb_2[Zn(H_2O)_6](SeO_4)_2$, x = 0.000			
100	2.121(1)	2.126(1)	2.039(1)	0.0019(5)	0.0022(5)	0.0014(5)
			$K_2[Zn(H_2O)_6](SeO_4)_2$, x = 1.000			
298	2.135(1)	2.128(1)	2.027(1)	0.0018(4)	0.0013(4)	0.0019(4)

Crystals found to be of high quality at room temperature and having suitable proportions of K^+ and Rb^+ were subsequently cooled below room temperature and data collected at several different temperatures to as low as 85 K. X-ray data for representative structures were measured both on the downward and upward parts of the temperature cycle. As discussed below, in the composition range ~32−41% K^+, the compound was found to change from form **B** to form **A** on cooling, with the temperature at which this occurred increasing as the proportion of K^+ decreased. In the region ~42−49% K^+, where the change occurred below ~200 K, several crystals were studied, and for most of these the R factors increased substantially for the low-temperature phase. In these cases, the R factors remained high when the structures were redetermined after warming the crystals, and the structures did not correspond to those observed before cooling. It appears that when the phase change occurs at low temperatures, it usually causes an irreversible degradation in crystal quality, and the results from these crystals are not included, *vide supra*.

Crystallographic data and structural refinements for 80 data sets belonging to $K_{2x}Rb_{2-2x}[Cu(H_2O)_6](SeO_4)_2$ (x = 0.0, 0.127, 0.262, 0.318, 0.359, 0.390, 0.411, 0.498, 0.729, and 1.0) and the isomorphous non-JT complexes, $K_2[Zn(H_2O)_6](SeO_4)_2$[25] and $Rb_2[Zn(H_2O)_6](SeO_4)_2$,[26] are summarized in Tables SA−SK, Supporting Information. Metal−oxygen bond lengths and differences in mean-square displacement amplitudes along M−O bonds, ΔU_{obs}(M−O) (Å^2; M = Cu and Zn), calculated from the anisotropic displacement parameters (ADP's) using PLATON for Windows, are given in Table 1. The structure of $K_2[Cu(H_2O)_6](SeO_4)_2$ is shown in Figure 2. The rubidium compound is isostructural and has the same atomic numbering scheme. Positional coordinates, bond lengths, bond angles, and anisotropic and isotropic displacement parameters for all 80 data sets are available in CIF format as Supporting Information.

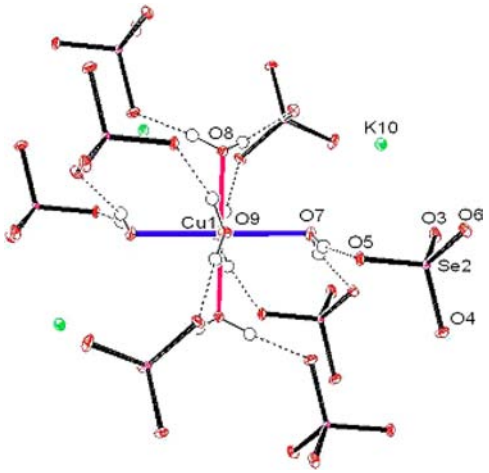

Figure 2. ORTEP drawing of the structure of $K_2[Cu(H_2O)_6](SeO_4)_2$ viewed approximately perpendicular to the short Cu−O(9) bond direction. Displacement ellipsoids are drawn at the 20% probability level. There are 12 hydrogen-bonding contacts for each $[Cu(H_2O)_6]^{2+}$ complex to eight surrounding selenate counteranions.

dx.doi.org/10.1021/ic401385f | *Inorg. Chem.* 2013, 52, 10481−10499

Table 2. (A) $O_{donor}\cdots O_{acceptor}$ Hydrogen-Bond Distances (Å) for $K_2[M(H_2O)_6](SeO_4)_2$ and $Rb_2[M(H_2O)_6](SeO_4)_2$ (M = Cu, Zn) at 298 K and (B) Eight Shortest X···O Distances (Å) in XO_n^+ Polyhedra for $K_2[M(H_2O)_6](SeO_4)_2$ and $Rb_2[M(H_2O)_6](SeO_4)_2$ (M = Cu, Zn) at 298 K

A

X	M	O(7)−H(15)···O(5)[a]	O(7)−H(16)···O(6)[b]	O(8)−H(17)···O(4)[c]	O(8)−H(18)···O(6)[d]	O(9)−H(19)···O(5)[e]	O(9)−H(20)···O(3)[f]
K	Cu	2.877(2)	2.831(2)	2.668(1)	2.720(1)	2.685(1)	2.654(1)
K	Zn	2.812(2)	2.824(2)	2.674(1)	2.741(1)	2.709(1)	2.673(1)
Rb	Cu	2.761(2)	2.772(2)	2.733(2)	2.763(3)	2.691(2)	2.678(2)
Rb	Zn	2.776(2)	2.803(2)	2.698(2)	2.741(2)	2.723(2)	2.684(2)

B

X	M	X(10)···O(3)[a]	X(10)···O(3)[b]	X(10)···O(4)[b]	X(10)···O(4)[c]	X(10)···O(5)[c]	X(10)···O(6)[d]	X(10)···O(7)[a]	X(10)···O(8)[e]	δ(Å)[f]
K	Cu	2.842(1)	2.992(1)	2.968(1)	3.496(1)	2.749(1)	2.794(1)	2.922(1)	3.023(1)	0.52
K	Zn	2.841(1)	2.974(1)	3.018(1)	3.424(1)	2.753(1)	2.815(1)	3.080(1)	2.979(1)	0.44
Rb	Cu	2.972(2)	3.070(2)	3.118(2)	3.211(2)	2.955(2)	2.949(2)	3.227(2)	3.069(2)	0.16
Rb	Zn	2.975(1)	3.016(1)	3.209(2)	3.335(2)	2.892(1)	2.946(1)	3.212(2)	3.131(1)	0.25

(A) Symmetry codes for acceptor atom O: [a] x, y, z. [b] $x, y, z-1$. [c] $x-1, y, z-1$. [d] $x-1/2, 1/2-y, z-1$. [e] $-x, -y, 1-z$. [f] $1/2-x, y-1/2, 1-z$. (B) Symmetry codes for atom O: [a] x, y, z. [b] $x-1/2, 1/2-y, z$. [c] $1/2-x, 1/2+y, 1-z$. [d] $x-1/2, 1/2-y, z-1$. [e] $1/2+x, 1/2-y, z$. [f] δ(Å) is the deviation of the longest of the eight X···O distances from the average.

Table 3. Distribution of Forms for Known Tutton's Salts $X_2[M(H_2O)_6](YO_4)_2$[a]

	$YO_4^{2-} = SeO_4^{2-}$						$YO_4^{2-} = SO_4^{2}$						
M X	K^+	Tl^+	Rb^+	NH_4^+	ND_4^+	Cs^+	Na^+	K^+	Tl^+	Rb^+	NH_4^+	ND_4^+	Cs^+
Mg^{2+}	**B**	**A**	**A**	**B**		**A**		A	**A**	**A**	**B**[b]	B	**A**
Cr^{2+}										**A**	**A**	**A**[c]	**A**
Mn^{2+}		**A**	**A**			**A**			**A**	**A**	**B**[b]	**B**	**A**
Fe^{2+}								**A**	**A**	**A**	**B**	**B**	**A**
Co^{2+}	**B**	**A**	**A**	**B**		**A**	**A**	**A**	**A**	**A**	**B**	**B**	**A**
Ni^{2+}	**B**	**A**	**A**	**B**	**B**	**A**		**A**	**A**	**A**	**B**	**B**	**A**
Cu^{2+}	**B**	**A**	**A**	**B**	**B**			**A**	**A**	**A**	**B**	**A**[c]	**A**
Zn^{2+}	**B**	**A**	**A**	**B**	**B**	**A**		**A**	**A**	**A**	**B**	**B**	**A**

[a] Form **A**: $d[M-O(8)] > d[M-O(7)]$. Form **B**: $d[M-O(7)] > d[M-O(8)]$. [b] Form **B** stable below ~160 K. [c] Form **B** stable at high pressure.

RESULTS AND DISCUSSION

Crystal Structures. Tutton's salts are a group of isomorphous compounds $X_2[M(H_2O)_6](YO_4)_2$ that crystallize in the monoclinic space group $P2_1/a$, $Z = 2$, with the $[M(H_2O)_6]^{2+}$ ion residing on an inversion center. The $[M(H_2O)_6]^{2+}$ ions are linked to four XO_n^+ polyhedra via the O(7) and O(8) waters and to eight surrounding YO_4^{2-} counteranions by hydrogen bonds to the six coordinated water molecules. The YO_4^{2-} counteranions, in turn, interact with the monovalent X cations (Figure 2). The six unique hydrogen-bond distances between the coordinated water O's and the selenate O's, O−H···O, and X···O distances within the XO_n^+ polyhedra for $K_2[Cu(H_2O)_6](SeO_4)_2$, $Rb_2[Cu(H_2O)_6](SeO_4)_2$, and their corresponding non-JT zinc analogues are given in Table 2A and B, respectively. Because the selenate O(3) and O(4) atoms accept only a single hydrogen bond, whereas O(5) and O(6) accept two, the former makes stronger hydrogen bonds to the coordinated waters than the latter, which is evident in Table 2A: O(8)−H(17)···O(4) < O(8)−H(18)···O(6) and O(9)−H(20)···O(3) < O(9)−H(19)···O(5).

The crystallographic site symmetry of the $[M(H_2O)_6]^{2+}$ ion in Tutton's salts is C_i, with the axial M−O(9) bonds equal in length and always shorter than the mean M−O bond length, which defines the direction of the tetragonal compression lattice strain in these structures. The site symmetry does not, however, require the M−O(7) and M−O(8) bonds to be equal in length, this being related to the orthorhombic component of the lattice strain. We adhere to the convention for the dimorphs that if $d[M-O(8)] > d[M-O(7)]$, $[M(H_2O)_6]^{2+}$ adopts form **A**; otherwise, it adopts form **B**, *vide supra*. The distribution of forms for all known Tutton's salts is given in Table 3. Aside from the tetrahedral NH_4^+ and ND_4^+ cations, which can form hydrogen (deuterium) bonds to the counteranions, all Tutton's salts with Tl^+, Rb^+, and Cs^+ adopt form **A** regardless of the M metal and the YO_4^{2-} counterion; in addition, all sulfate Tutton's salts with monatomic cations adopt form **A** regardless of M.

The reason why a $[M(H_2O)_6]^{2+}$ ion in a Tutton's salt crystal adopts a particular form is not immediately obvious, but a close inspection of the data in Table 2B provides some clues. The eight shortest X···O distances in the XO_n^+ coordination polyhedra for $K_2[Cu(H_2O)_6](SeO_4)_2$, $Rb_2[Cu(H_2O)_6](SeO_4)_2$, and their zinc analogues are listed; by taking the average of these distances and subtracting it from the longest distance, we get a deviation labeled δ.[27] For $K_2[Cu(H_2O)_6](SeO_4)_2$ and its zinc analogue, the δ values are relatively large, 0.52 and 0.44 Å, whereas for $Rb_2[Cu(H_2O)_6](SeO_4)_2$ and its zinc analogue, they are only 0.16 and 0.25 Å. Thus, the relatively large δ values for the K^+ polyhedra suggest that K^+ should be best classified as 7-fold coordinate, compared with the smaller δ values for the larger Rb^+ cation, which is 8-fold coordinate.[28] Including data for the other selenate Tutton's salts given in Supporting Information S1A, we see that Tl^+ is also 8-fold coordinate, while the larger Cs^+ cation is 9-fold coordinate.[29] This analysis can be extended to the sulfate Tutton's salts: for $K_2[Cu-$

dx.doi.org/10.1021/ic401385f | Inorg. Chem. 2013, 52, 10481−10499

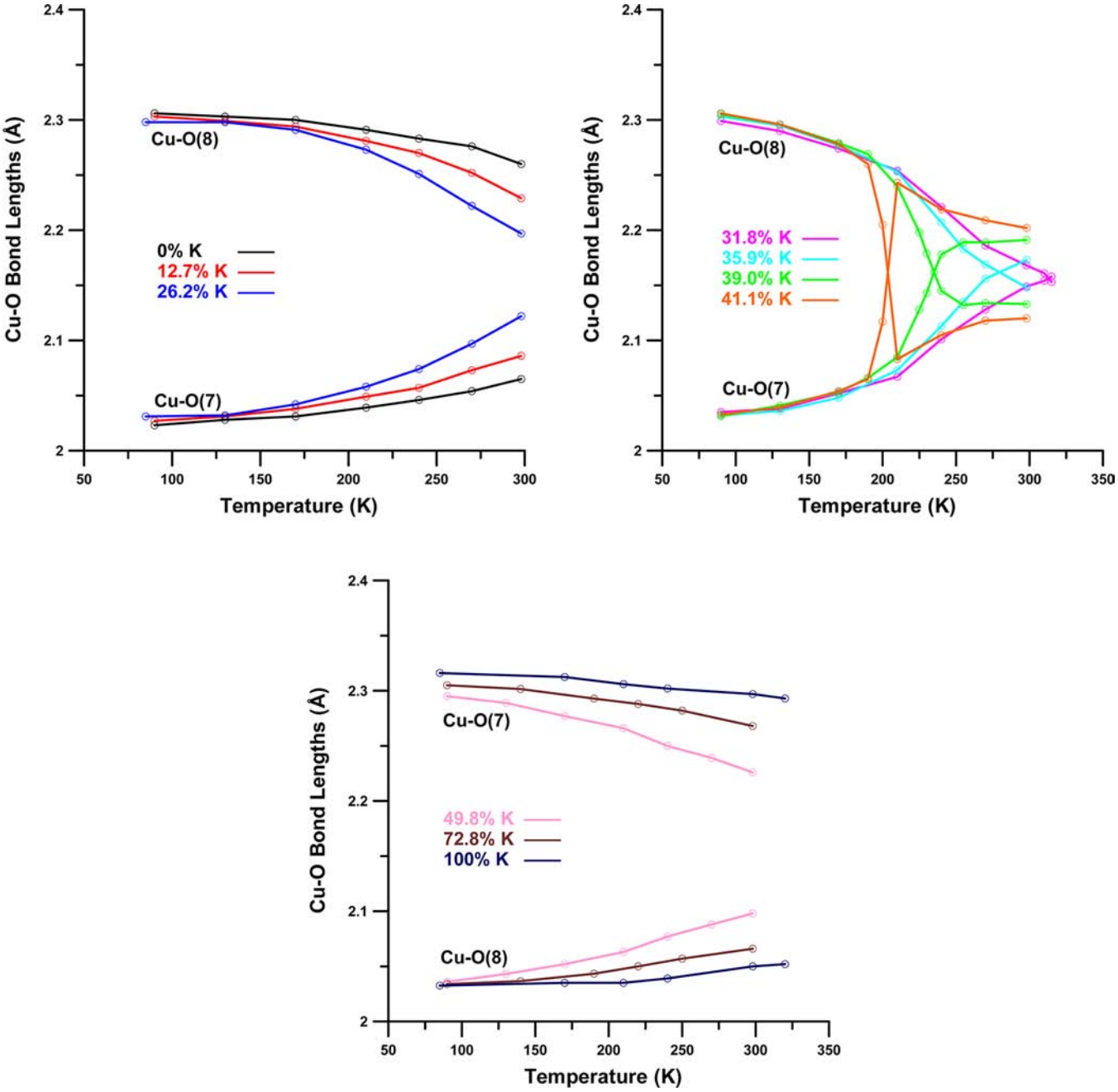

Figure 3. Temperature dependence of Cu−O(7) and Cu−O(8) bond lengths for crystals of $K_{2x}Rb_{2-2x}[Cu(H_2O)_6](SeO_4)_2$ with 0, 12.7 and 26.2 (left); 31.8, 35.9, 39.0, and 41.1 (right); and 49.8, 72.8, and 100% K (bottom). Crystals with compositions 0.0, 12.7, and 26.2% K^+ have the structure of form **A** at all temperatures, those with compositions 49.8, 72.8, and 100% K^+ have form **B**, whereas those with intermediate compositions 31.8, 35.9, 39.0, and 41.1% K^+ switch from form **B** above the transition temperature to form **A** below; the transition temperatures are 312, 280, 235, and 205 K, respectively, at which the crystallographically determined Cu−O(7) and Cu−O(8) bond lengths are equal.

$(H_2O)_6](SO_4)_2$ and its zinc analogue, the δ values are only 0.20 and 0.31 Å, whereas for $Rb_2[Cu(H_2O)_6](SO_4)_2$ and its zinc analogue, they are 0.19 and 0.16 Å. These values are similar, indicating that for the sulfate Tutton's salts, K^+, like Rb^+ and Tl^+, is 8-fold coordinate,[30] while Cs^+ can be shown to be 9-fold coordinate (Supporting Information S1B).[31,32] These observations are consistent with the relative sizes of the cations/anions: K^+ is much smaller relative to SeO_4^{2-} and can achieve only 7-fold coordination, whereas 8-fold coordination is possible with the smaller SO_4^{2-}. The larger cations match up well with either counteranion and can achieve 8- or even 9-fold coordination. In conclusion, $[M(H_2O)_6]^{2+}$ ions in Tutton's salts with monatomic cations that are 8- or 9-fold coordinate adopt form **A**; otherwise, they adopt form **B**.[33]

The tendency of K^+ and Rb^+ to achieve 7- and 8-fold coordination in $K_2[M(H_2O)_6](SeO_4)_2$ (form **B**) and $Rb_2[M(H_2O)_6](SeO_4)_2$ (form **A**) Tutton's salts, respectively, results in SeO_4^{2-} groups with different orientations with respect to the cations and to the coordinated waters of the $[M(H_2O)_6]^{2+}$ ions in the two forms. As a consequence, the strength of the O−H···O hydrogen-bonding interactions with the O(7) and O(8) waters will be different in the two structures, as will the net interactions along the M−O(7) and M−O(8) bonds, the inequality of which is a direct measure of the orthorhombic

strain.[9,16] We shall, therefore, analyze the orthorhombic strain simply in terms of the interaction of the M−O(7) and M−O(8) waters with the eight surrounding SeO_4^{2-} groups, ignoring the much weaker M−O(7) and M−O(8) interactions with the X cations,[33] using a simple crystallographic model for the non-JT Tutton's salts based on a phenomenological parameter labeled Δ. This parameter is defined as the *difference* between the average of the two $O_{donor}\cdots O_{acceptor}$ distances involving O(7) [O(7)−H(15)···O(5) and O(7)−H(16)···O(6)], and the average of the two involving O(8) [O(8)−H(17)···O(4) and O(8)−H(18)···O(6)], i.e., Δ (Å) ≡ [O(7)−H(15)···O(5) + O(7)−H(16)···O(6)]/2 − [O(8)−H(17)···O(4) + O(8)−H(18)···O(6)]/2. Using high-quality literature data and the results obtained in this X-ray diffraction laboratory (C.J.S.), Δ values have been determined in this manner; see Supporting Information 2A and 2B. The results group together according to the X cations and are rather insensitive to the nature of the M ions, creating a gap in the spectrum of values that separates form **B** structures from form **A** ones.[34] For example, the average Δ values for the potassium and rubidium non-JT selenate Tutton's salts are 0.109(3) Å (form **B**) and 0.070(7) Å (form **A**), respectively.[35]

The variation of the Cu−O(7) and Cu−O(8) bond lengths as a function of temperature and the amount of K^+ dopant for the mixed $K_{2x}Rb_{2-2x}[Cu(H_2O)_6](SeO_4)_2$ crystals is shown in Figure 3; Cu−O(9) bond lengths are temperature independent and are not shown. The pure Rb^+ (0% K^+) salt and those with 12.7 and 26.2% K^+ adopt form **A** at all temperatures (Figure 3; left), while the pure K^+ salt and that with 49.8 and 72.8% K^+ exist in form **B** over the whole temperature range (Figure 3; bottom). However, it is seen that in the range of ∼32−41% K^+ the two forms switch with a change of temperature which varies between 298 K (33% K^+) and 205 K (41% K^+) (Figure 3; right). For these K^+/Rb^+ mixed crystals, a weighted average for Δ could be identified and calculated using the average Δ values for the pure K^+ and Rb^+ non-JT selenate salts (Δ = 0.109 and 0.070 Å for K^+ and Rb^+, respectively) and the relative amount of the dopant. Thus, for a K^+ dopage in the range 33−41%, Δ is calculated to be 0.083−0.086 Å. For a mixed $K_{2x}Rb_{2-2x}[Zn(H_2O)_6](SeO_4)_2$ crystal with 54% K^+, in which Zn−O(7) = 2.127(2) and Zn−O(8) = 2.120(2) Å (data not shown; form **B**), the observed Δ value is 0.091 Å (Supporting Information 2A),[36] exactly that predicted using the weighted-average values for the pure K^+ and Rb^+ non-JT selenate Tutton's salts: 0.54(0.109 Å) + 0.46(0.070 Å) = 0.091 Å. Thus, it appears possible to systematically modulate the energy difference between the two lowest minima of the ground-state adiabatic potential energy surface for the $[Cu(H_2O)_6]^{2+}$ ion in mixed K^+/Rb^+ crystals by simply varying the relative amount of the dopant.

Another factor that influences the energy difference between the potential energy minima of the $[Cu(H_2O)_6]^{2+}$ ion in Tutton's salts and correspondingly the temperature dependence of its Cu−O bond lengths is the cooperative JT interactions between Cu^{2+} centers.[37] As shown in Figure 4, $[Cu(H_2O)_6]^{2+}$ ions stack in such a manner that the Cu−O(7) and Cu−O(8) bonds involved in the thermal equilibrium lie nearly in the *ab* plane of the unit cell. If a $[Cu(H_2O)_6]^{2+}$ ion located at a corner of the unit cell has its *longest* Cu−O bond pointed toward the center, then the $[Cu(H_2O)_6]^{2+}$ ion on the corner diagonal to it has the same arrangement, whereas the diagonals of the other two $[Cu(H_2O)_6]^{2+}$ ions on the unit cell corners have their *intermediate* Cu−O bonds pointed toward

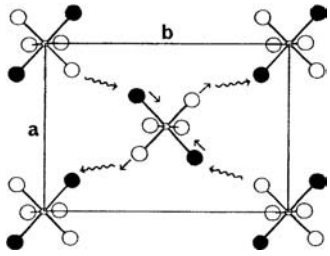

Figure 4. Schematic illustration of the cooperative interactions resulting from thermal excitation of a central $[Cu(H_2O)_6]^{2+}$ ion in $K_{2x}Rb_{2-2x}[Cu(H_2O)_6](SeO_4)_2$ Tutton's salts. The view is a projection onto the *ab* plane along the *c* axis of the unit cell, approximately parallel to the temperature-independent Cu−O(9) bonds; cations and counter SeO_4^{2-} anions are not shown. The antiferrodistortive arrangement of the temperature-dependent long and intermediate Cu−O bonds of the central $[Cu(H_2O)_6]^{2+}$ ion and four neighbors, which all lie approximately in the *ab* plane, is shown by blackened atoms representing long Cu−O bonds and open circles representing intermediate and short Cu−O bonds.

the center. This antiferrodistortive arrangement of Cu−O bonds in Tutton's salts has two of the *longest* Cu−O bonds at opposite corners of the unit cell oriented approximately parallel to the *intermediate* Cu−O bonds of the central $[Cu(H_2O)_6]^{2+}$ ion, and two of the *intermediate* Cu−O bonds at the other opposite corners oriented approximately parallel to the *longest* Cu−O bonds of the central $[Cu(H_2O)_6]^{2+}$ ion. If, say, the central JT $[Cu(H_2O)_6]^{2+}$ ion in the unit cell of Figure 4 is thermally excited, then the lengthening of its *intermediate* bonds will increase the strain acting along the *longe*st Cu−O bonds of two diagonal neighbors, while the concomitant shortening of its *longest* Cu−O bonds will reduce the compression acting on the *intermediate* bonds of the other two diagonal neighbors; thus, both effects try to even the bond lengths of the corner $[Cu(H_2O)_6]^{2+}$ ions. As these interactions are cooperative in nature, being transmitted via the hydrogen-bonding network throughout the whole crystal, the orthorhombic lattice strain is effectively reduced, and the energy difference between the two minima of the potential energy surface is decreased.[11] The decrease in orthorhombic strain with increasing temperature as a result of cooperative interactions in JT Tutton's salts is well-known in general (*vide infra*).[11,17,38,39]

Complementary to Figure 3 are plots of Cu−O(7) and Cu−O(8) bond lengths as a function of K^+ concentration for 298, 270, 240, 210, 170, 130, and 90 K isotherms for mixed K^+/Rb^+ crystals in Figure 5 (left). They show that only form **A** exists from 0 to 33% K^+, whereas only form **B** exists from 45 to 100% K^+, at least at temperatures below room temperature. Transitions between the two forms are possible, however, in the zone indicated by dashed vertical lines in Figure 5 (left). Starting with pure $Rb_2[Cu(H_2O)_6](SeO_4)_2$ (K^+ = 0%) and progressively adding K^+, transitions occur beginning at 33% K^+ and ending at 45% K^+, in theory, although this limit may be crystallographically inaccessible due to the formation of domains and poor crystal quality. The corresponding weighted Δ value, ∼0.088 Å, represents the cutoff value that separates forms **A** and **B** which occurs at zero orthorhombic strain, i.e., equal Cu−O(7) and Cu−O(8) bond lengths. Transitions beginning at the lower-end of the zone (Δ = 0.083 Å) can still occur, albeit at higher temperatures, because cooperative JT interactions essentially lower the orthorhombic strain vis-à-vis that calculated with the Δ model, which uses data for non-JT

dx.doi.org/10.1021/ic401385f | *Inorg. Chem.* 2013, 52, 10481−10499

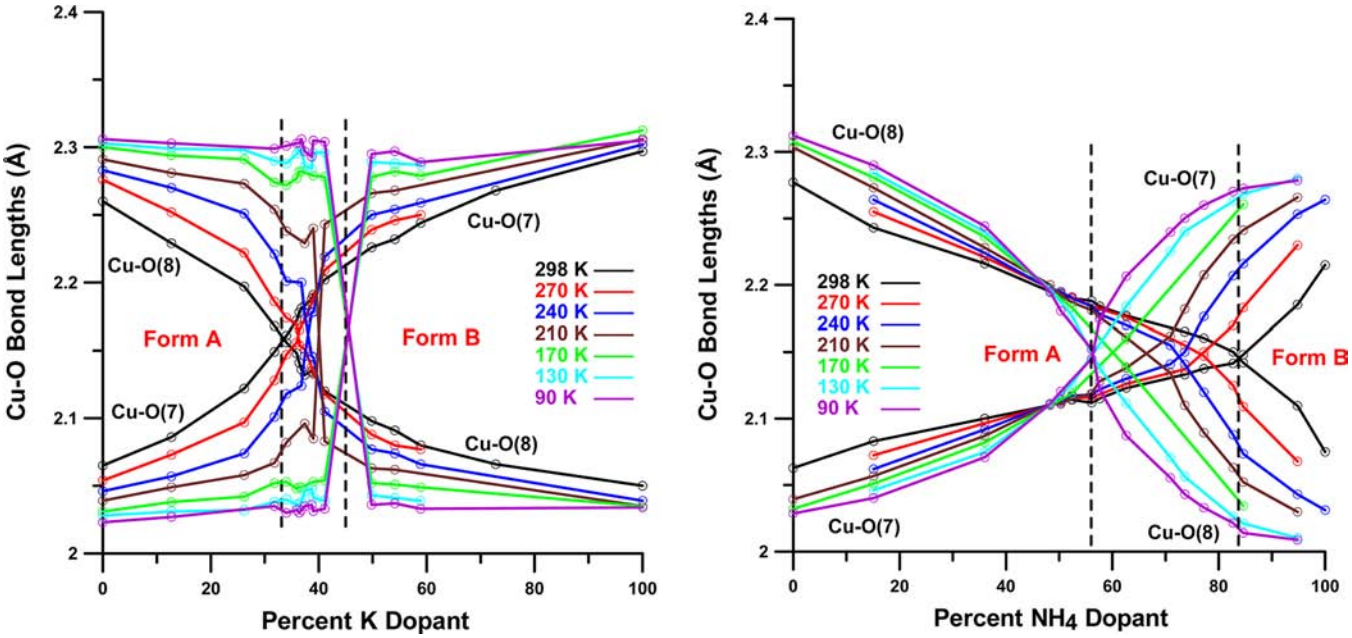

Figure 5. Left. Plots of Cu−O(7) and Cu−O(8) bond lengths as a function of percent K^+-dopant concentrations for 298, 270, 240, 210, 170, 130, and 90 K isotherms for mixed $K_{2x}Rb_{2-2x}[Cu(H_2O)_6](SeO_4)_2$ crystals. The vertical dashed lines separate regions where only form **A** (left; 0−33% K^+) and form **B** (right; 45−100% K^+) structures exist at temperatures less than room temperature; transitions between the two forms are possible within the zone between the two extreme regions. The consistency of the data is demonstrated by the fact that the Cu−O(7) and Cu−O(8) bond lengths intersect at virtually the same value (2.16 Å) at the transition points. Right. Plots of Cu−O(7) and Cu−O(8) bond lengths as a function of percent NH_4^+-dopant concentrations for 298, 270, 240, 210, 170, 130, and 90 K isotherms for mixed $(NH_4)_{2x}K_{2-2x}[Cu(H_2O)_6](SO_4)_2$ crystals. The vertical dashed lines separate regions where only form **A** (left; 0−56% NH_4^+) and form **B** (right; 84−100% NH_4^+) structures exist at less than room temperature.

complexes (no cooperativity), compensating for the extra 0.05 Å needed to reach the cutoff value of 0.088 Å. Conversely, starting with a crystal of $K_2[Cu(H_2O)_6](SeO_4)_2$ and substituting Rb^+, and noting that pure $Rb_2[Cu(H_2O)_6](SeO_4)_2$ has less orthorhombic strain, transitions begin at 45% K^+ (55% Rb^+) at ∼170 K; with the addition of more Rb^+ and increasingly stronger cooperative interactions at higher temperatures, the cutoff value of 67% Rb^+ (Δ = 0.083 Å) for the **B** → **A** transition is reached.[40]

It is also seen from Figures 3 and 5 (left) that the Cu−O(7) and Cu−O(8) bond lengths of pure $Rb_2[Cu(H_2O)_6](SeO_4)_2$ show a greater temperature dependence than those of pure $K_2[Cu(H_2O)_6](SeO_4)_2$; this is completely consistent with the Δ model, as the size of orthorhombic strain is proportional to the deviation from either the cutoff value of 0.086 Å for (**A** → **B**) or 0.083 Å for (**B** → **A**). That is, $\Delta(Rb^+)$ = 0.070 Å is closer to 0.086 Å than $\Delta(K^+)$ = 0.109 Å is to 0.083 Å.[41] A consequence of this is that the transition zone is shifted to the left of the midpoint along the K^+-dopant concentration axis; form **A** is the most stable form at low temperatures within the transition zone. Also shown in Figure 5 (right) is a similar plot for the related mixed series of $(NH_4)_{2x}K_{2-2x}[Cu(H_2O)_6](SO_4)_2$ crystals;[43] notice that the two plots are approximately mirror images of each other. In this case, $(NH_4)_2[Cu(H_2O)_6](SO_4)_2$ (form **B**) shows a greater temperature variation of its Cu−O(7) and Cu−O(8) bond lengths than does $K_2[Cu(H_2O)_6](SO_4)_2$ (form **A**), and the transition zone is shifted to the right of the midpoint of the NH_4^+-dopant concentration axis. Form **B** is now the most stable form at low temperatures in the transition zone. This is interesting, because in Cu^{2+}-doped $X_2[Zn(H_2O)_6](SO_4)_2$ crystals (X = K^+ and NH_4^+) it is the K^+ complex that shows a greater temperature dependence of its EPR *g* values than the corresponding NH_4^+ complex.[42] This reversal may be because cooperative JT interactions in a pure crystal of $(NH_4)_2[Cu(H_2O)_6](SO_4)_2$ are much stronger than in $K_2[Cu(H_2O)_6](SO_4)_2$ because of the extensive hydrogen-bonding network in the former complex; in a doped crystal, these interactions are disrupted and the smaller eight-coordinate K^+-cation complex has less orthorhombic strain.[44]

That the cooperative JT interactions are significantly stronger and the orthorhombic strain concomitantly much lower in the mixed NH_4^+ complex can also be inferred from Figure 5 (right), where it is seen that **B** → **A** transitions in $(NH_4)_{2x}K_{2-2x}[Cu(H_2O)_6](SO_4)_2$ extend from 298 (16% K^+) to 90 K (44% K^+), in contrast to $K_{2x}Rb_{2-2x}[Cu(H_2O)_6](SeO_4)_2$, where they occur only above ∼170 K (Figure 5; left). Interestingly, in mixed crystals of $(NH_4)_{2x}Rb_{2-2x}[Cu(H_2O)_6](SO_4)_2$, the **B** → **A** transition occurs with the addition of only 9% Rb^+ to pure $(NH_4)_2[Cu(H_2O)_6](SO_4)_2$ instead of 16% K^+ in $(NH_4)_{2x}K_{2-2x}[Cu(H_2O)_6](SO_4)_2$ at ambient temperature, a direct manifestation of the greater orthorhombic strain present in the Rb-sulfate crystal than in the K-sulfate crystal.[43]

The results shown in Figure 5 can also be thought of from a thermodynamical perspective. For the **A** → **B** phase transitions in the mixed series of $K_{2x}Rb_{2-2x}[Cu(H_2O)_6](SeO_4)_2$ complexes, ΔH is probably positive, as the Rb^+ cation is 8-fold coordinate in $Rb_2[Cu(H_2O)_6](SeO_4)_2$ (form **A**), whereas K^+ is only 7-fold coordinate in $K_2[Cu(H_2O)_6](SeO_4)_2$ (form **B**). Therefore, more X···O interactions have to be broken than are reformed in the transition. It seems likely that ΔS is also positive, as 7-fold cation coordination and greater dopant concentration implies more disorder and hence a higher entropy than 8-fold cation coordination and less dopant. Transitions occur beginning at 33% K^+ and 298 K with ΔH

dx.doi.org/10.1021/ic401385f | *Inorg. Chem.* 2013, 52, 10481−10499

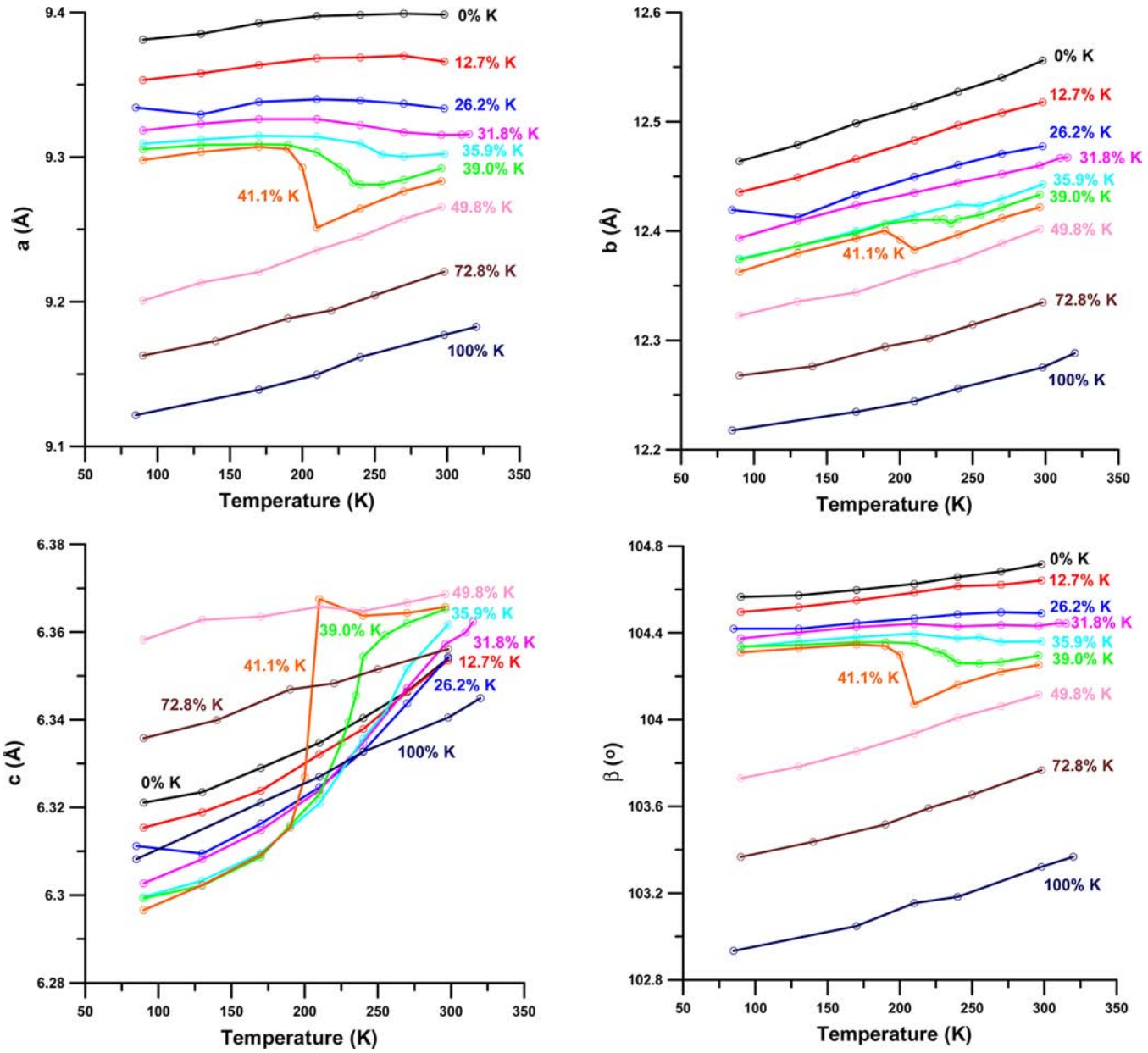

Figure 6. Plots of unit cell parameters for mixed crystals of $K_{2x}Rb_{2-2x}[Cu(H_2O)_6](SeO_4)_2$ with 0, 12.7, 26.2, 31.8, 35.9, 39.0, 41.1, 49.8, 72.8, and 100% K^+ as a function of temperature. Beginning at about 180−250 K for complexes within the 32−41% K^+ transition zone, *a*, *b* and *β* start to contract and *c* expands rapidly, reflecting the first-order **A** → **B** phase transitions which occur at 205 K (41.1% K^+), 235 K (39.0% K^+), 280 K (35.9% K^+), and 312 K (31.8% K^+).

becoming less positive with increasing amounts of K^+ dopant, requiring $-T\Delta S$ to become less negative in order for $\Delta G = \Delta H - T\Delta S$ to be zero, which is accomplished by lower transition temperatures and/or slightly decreasing values of ΔS. For the opposite transitions, **B** → **A**, ΔH and ΔS are both negative; transitions begin at 55% Rb^+ at ∼170 K, i.e., at relatively low temperatures in order to minimize the positive value of $-T\Delta S$. ΔH becomes increasingly more negative with increasing amounts of Rb^+, requiring higher transition temperatures with correspondingly larger positive $-T\Delta S$ values. For the mixed series of $(NH_4)_{2x}K_{2-2x}[Cu(H_2O)_6](SO_4)_2$ complexes, **B** → **A** transitions occur beginning at 16% K^+ and 298 K. ΔH is also positive because of the relatively large amount of energy required to break up the extensive H-bonding network in pure $(NH_4)_2[Cu(H_2O)_6](SO_4)_2$, and ΔS is positive; accordingly, the **B** → **A** and **A** → **B** transitions are analogous to the **A** → **B** and **B** → **A** transitions for $K_{2x}Rb_{2-2x}[Cu(H_2O)_6](SeO_4)_2$ complexes, respectively.

It was noted above that within the region of 42−49% K^+ for the mixed $K_{2x}Rb_{2-2x}[Cu(H_2O)_6](SeO_4)_2$ complexes, crystal quality was generally good at temperatures above ∼170 K, below which the quality deteriorated rapidly. In light of the discussion above, these observations are consistent with the idea that within this doping region, strong cooperative JT interactions at temperatures slightly greater than ∼170 K cause clusters of form **B** structures to separate from those of form **A**, resulting in domains located inhomogeneously throughout the crystal and a metastable "frozen" crystalline state that remains locked-in even if the temperature of the crystal is lowered below ∼170 K. It should be mentioned that domain separation

dx.doi.org/10.1021/ic401385f | *Inorg. Chem.* 2013, 52, 10481−10499

was observed in a synchrotron X-ray diffraction/Bragg peak-shape analysis of an 85% deuterated mixed single crystal of $(ND_4/NH_4)_2[Cu(D_2O)_6](SO_4)_2$ at 12 K, essentially disappearing at 320 K.[46] Fluctuating domains in pure $(ND_4)_2[Cu(D_2O)_6](SO_4)_2$ were also predicted to occur in a two-dimensional lattice using a statistical model of cooperative JT coupling.[11,47,48]

Plots of the unit cell parameters *a*, *b*, *c*, and β as a function of temperature and percent K^+ dopant are shown in Figure 6. Overall, the unit cell volume shows a gradual, steady increase as the larger Rb^+ replaces K^+ (Figure 1). At low temperatures, all three axes expand as the temperature rises, as expected for a normal crystal. However, beginning at about 180−250 K for complexes within the 32−41% K^+ transition zone, *a*, *b*, and β start to contract and *c* expands rapidly, reflecting the switch in directions of the long and intermediate Cu−O bonds in the **A** → **B** transition. This same pattern is also observed upon warming pure $(ND_4)_2[Cu(D_2O)_6](SO_4)_2$[2] and for its pressure-induced phase change to form **B** at 15 K and a pressure of 1.5 kbar[4] and for other combinations of temperature and pressure,[7,8] by doping copper with small amounts of zinc in $(ND_4)_2[Cu_{1-x}Zn_x(D_2O)_6](SO_4)_2$[6] and $(NH_4)_2[Cr_{1-x}Zn_x(H_2O)_6](SO_4)_2$,[14] and by warming pure $(NH_4)_2[Cr(H_2O)_6](SO_4)_2$.[39] It should also be noted that the density differences between the two forms in the mixed K^+/Rb^+ crystals are relatively small. For example, in $K_{2x}Rb_{2-2x}[Cu(H_2O)_6](SeO_4)_2$ with 41.1% K^+, a transition occurs at 205 K: form **A** has a density of 2.777 g/cm^3 at 200 K, and form **B** has a density of 2.771 g/cm^3 at 210 K, only a 0.2% difference, Table S-G Supporting Information. For the mixed series of $(NH_4)_{2x}K_{2-2x}[Cu(H_2O)_6](SO_4)_2$ and $(NH_4)_{2x}Rb_{2-2x}[Cu(H_2O)_6](SO_4)_2$ complexes, the **B** → **A** transitions have density changes of less than 0.1% and go from lower to higher density.[43] The small change in density observed[6] at room temperature near the transition of form **A** (x = 0.013), 2.020 g/cm^3 (V = 690.4 Å^3), to form **B** (x = 0.034), 2.029 g/cm^3 (V = 687.9 Å^3), induced by adding small amounts of zinc to mixed $(ND_4)_2[Cu_{1-x}Zn_x(D_2O)_6](SO_4)_2$ complexes, is less than ∼0.4%. These results suggest that nonpressure, substitutional-induced phase changes in mixed JT Tutton's salts do not involve significant changes of the densities of the two phases (forms).

Pressure-induced phase changes and structural transitions have been observed in pure $(ND_4)_2[Cu(D_2O)_6](SO_4)_2$ (form **A**) as mentioned and $(ND_4)_2[Cr(D_2O)_6](SO_4)_2$ (form **A**).[13] For example, an **A** → **B** transition in $(ND_4)_2[Cu(D_2O)_6](SO_4)_2$ was observed at 15 K and 1.5 kbar of pressure;[4] form **A** (1.989 g/cm^3 at 15 K and 1 bar) has a significantly lower density compared with form **B** (2.032 g/cm^3 at 15 K and 1.5 kbar),[4] a 2% difference. However, at 260 K and ∼1.2 kbar of pressure, form **A** (∼ 2.020 g/cm^3) switches to form **B** (∼ 2.035 g/cm^3), and a 0.7% difference was observed, whereas at 303 K and ∼200 bar, only a 0.3% difference occurred.[8] Thus, the density changes in $(ND_4)_2[Cu(D_2O)_6](SO_4)_2$ induced by pressure appear to depend on the temperature and magnitude of the hydrostatic pressure. Interestingly, efforts to pressure-switch $K_2[Cu(H_2O)_6](SO_4)_2$[7] and $Rb_2[Cr(D_2O)_6](SO_4)_2$[13] from **A** → **B** with 1.4 kbar (at 15 K) and 7.5 kbar (at 10 K) of pressure, respectively, were unsuccessful; this is not surprising, as form **A** is the most stable form adopted by sulfate Tutton's salts with monatomic cations, and switching to the less stable form **B** would be extremely unlikely.[49] As a side note, we are unaware of any experiments having been conducted at high pressure, using either EPR or X-ray diffraction techniques, involving a JT-$X_2[M(H_2O)_6](YO_4)_2$ Tutton's salt crystal with mixed compositions for X and/or Y. Presumably, for $K_{2x}Rb_{2-2x}[Cu(H_2O)_6](SeO_4)_2$ crystals close to the transition composition on the low density side, such pressure switching between the **B** → **A** forms may occur.

Vibronic Coupling Model and the Potential Surface of the $[Cu(H_2O)_6]^{2+}$ Ion. An important consideration for the present series of compounds is the nature of the potential surface of the $[Cu(H_2O)_6]^{2+}$ ion and the way in which this is influenced by JT coupling and interactions with the surrounding crystal lattice. The deviation from a regular octahedral geometry of a complex distorted by $E_g \otimes e_g$ JT coupling is described in terms of the two components Q_θ and Q_ε of the JT active e_g vibration.[50] The displacements and the corresponding composition of the electronic part of the ground state wave function, Ψ_e, can also be expressed in terms of polar coordinates

$$Q_\theta = \rho \cos\phi \quad Q_\varepsilon = \rho \sin\phi \tag{1a}$$

$$\Psi_e = d_{x^2-y^2} \cos(\phi/2) + d_{z^2} \sin(\phi/2) \tag{1b}$$

For a complex with six identical ligands, the distortion is driven by the linear coupling constant A_1 forming the so-called "Mexican hat" potential surface. At this level of approximation, the energy minimum is a circular well of radius ρ_o, and the geometry fluctuates between various conformations of D_{4h} and D_{2h} symmetry that are generated by linear combinations of Q_θ and Q_ε as ϕ is varied. Higher-order coupling effects, represented by the parameter A_2, cause a "warping" of the potential surface to give three equivalent minima at ϕ = 0, 120, and 240° for $A_2 > 0$ corresponding to tetragonal elongations with a $d_{x^2-y^2}$ type ground state, and three saddle points at ϕ = 60, 180, and 300° corresponding to tetragonal compressions. The extent of the warping is normally expressed by the parameter $\beta \sim A_2(A_1/h\nu_{JT})^2$, the energy difference between the minima and saddle points being given by 2β. When the site symmetry is low, such as C_i for the $[Cu(H_2O)_6]^{2+}$ ion in Tutton's salts, the geometry of the complex is also influenced by the strain imposed on it by the surrounding lattice, so that the three minima are no longer equal in energy.

The general form of the "warped Mexican-hat" potential energy surface can therefore be parametrized using the first (A_1) and second (A_2) order JT coupling constants, the wavenumber of the JT active e_g vibrational mode of the hypothetical undistorted octahedral complex ($h\nu_{JT}$), and the axial (S_θ) and orthorhombic (S_ε) components of the strain imposed by the lattice. The approximation is made here that the strain term does not destroy the symmetry of the cubic part of the Hamiltonian. The adiabatic potential energy surface is given by[51]

$$E^{\pm} = h\nu_{JT}(Q_\theta^2 + Q_\varepsilon^2)/2 \pm [(A_1Q_\theta + A_2(Q_\theta^2 - Q_\varepsilon^2) + S_\theta)^2 + (A_1Q_\varepsilon - 2A_2Q_\theta Q_\varepsilon + S_\varepsilon)^2]^{1/2} \tag{2}$$

where the anharmonicity of the tetragonal component of the e_g vibration (Q_θ) has been neglected. The various parameters are conventionally given in units of cm^{-1}, except for the coordinates Q_θ and Q_ε, which are dimensionless.

The complexes for which the potential surfaces have been defined most accurately are those exhibiting dynamic equilibria

involving the direction of the JT distortion. Such behavior has been observed for many copper(II) complexes,[15] being first interpreted correctly in a pioneering study by Silver and Getz of the EPR spectrum of the $[Cu(H_2O)_6]^{2+}$ ion in Cu^{2+}-doped $K_2[Zn(H_2O)_6](SO_4)_2$.[52] In this approach, termed the SG model, it was shown that the temperature variation of the observed g values could be interpreted satisfactorily in the presence of small strains by assuming a thermal equilibrium between two complexes differing solely by the interchange of the directions of the long and intermediate bonds and their associated g values. The basic assumption of this approach has been confirmed for several complexes,[53] including $(ND_4)_2[Cu(D_2O)_6](SO_4)_2$[38] using Extended X-ray Absorption Fine Structure (EXAFS).

The "warped Mexican hat" potential surfaces of various complexes of the above kind have been derived in an approach developed by Riley et al., the RHW model.[42] This was used to describe the temperature variation of the g values of Cu^{2+} doped into a range of salts[42,54,55] and has been extended to include the temperature dependence of the average metal−ligand bond lengths and thermal ellipsoid parameters observed in X-ray and neutron diffraction,[51] as well as the situation where all three average g values change as a function of temperature.[55] Most recently, the RHW model was used to determine the way in which the potential surface of the $[Cu(H_2O)_6]^{2+}$ ion depends upon composition in the mixed-crystal series $K_2[Cu(H_2O)_6](SO_4)_{2-2x}(SeO_4)_{2x}$,[20] and the method described in detail for this system is applied to the present compounds.

To apply the RHW model to $[Cu(H_2O)_6]^{2+}$ ions in $K_{2x}Rb_{2-2x}[Cu(H_2O)_6](SeO_4)_2$ crystals and calculate the potential energy surfaces and vibronic wave functions and energy levels, the JT coupling parameters, $h\nu_{JT}$, A_1, and A_2, and strain parameters, S_θ and S_ε, must be determined from experiment. This was done first for the pure $Rb_2[Cu(H_2O)_6](SeO_4)_2$ and $K_2[Cu(H_2O)_6](SeO_4)_2$ compounds by systematically adjusting the parameters to minimize the differences between calculated and observed temperature dependent Cu−O bond lengths; the resulting optimized parameters are given in Table 4 and corresponding fits shown in Figure 7. It should be noted that the energy of the JT e_g vibrational mode, $h\nu_{JT}$, was not varied in the data optimization but was fixed at 258 cm^{-1}, which corresponds to the average energy of the a_g doublets of the split e_g vibration observed for several zinc(II) hexahydrated ions in different lattices.[56] Although its value is lower than that used in the previous analyses of the EPR spectra of the $[Cu(H_2O)_6]^{2+}$ ion, 300 cm^{-1},[42] it is very similar to the value (254 cm^{-1}) used for the analysis of Cr−O bond lengths for the JT $(NH_4)_2[Cr(H_2O)_6](SO_4)_2$ complex.[39] Gratifyingly, our best-fit values for A_1 = 940 cm^{-1} and A_2 = 13 cm^{-1} are the same for both complexes. Our value of A_1 is similar to that found (900 cm^{-1}) in studies of the temperature dependence of the EPR spectra of Cu^{2+}-doped zinc(II) Tutton's salts[42] and of the bond lengths of $(NH_4)_2[Cr(H_2O)_6](SO_4)_2$;[39] a value of 1100 cm^{-1} was derived from an EXAFS study of $(ND_4)_2[Cu(D_2O)_6](SO_4)_2$,[38] while an average estimate of 960 cm^{-1} was reported by Bill[57] for a range of copper(II) oxygen complexes. The value for the warping parameter, β = 173 cm^{-1} (A_2 = 13 cm^{-1}), is lower than previous estimates of ∼300 cm^{-1} [42] and 225 cm^{-1} [55] for the $[Cu(H_2O)_6]^{2+}$ ion; however, these values were not determined using a data-fitting algorithm and are less reliable. For the mixed K^+/Rb^+ complexes, values for $h\nu_{JT}$ (258 cm^{-1}), A_1 (940 cm^{-1}), and A_2 (13 cm^{-1}) were chosen to be the same as the pure complexes in determining the optimized strain parameters, S_θ and S_ε, which are given in Table 4 for all complexes. Note, for those complexes (32−41% K^+) that undergo **A** → **B** transitions, the data were analyzed only in the low-temperature, form **A** regions.

Within the framework of the RHW model, the parameters S_θ and S_ε represent the strain acting on the hypothetical octahedral $[Cu(H_2O)_6]^{2+}$ complex in the absence of vibronic coupling effects. Such strain parameters would be expected to occur in the corresponding isomorphous non-JT zinc(II) Tutton's salt complexes and result in the observed tetragonal and orthorhombic distortions of the $[Zn(H_2O)_6]^{2+}$ ion. The following equations allow rough estimates of S_θ and S_ε from the Zn−O bond lengths given in Table 1 for $Rb_2[Zn(H_2O)_6](SeO_4)_2$ and $K_2[Zn(H_2O)_6](SeO_4)_2$:[20]

$$S_\theta = 0.1722A_1(d_z - d_o)\sqrt{3}\sqrt{Mh\nu} \quad (3)$$

$$S_\varepsilon = 0.1722A_1(d_x - d_y)\sqrt{Mh\nu} \quad (4)$$

where M = 18 amu (H_2O); $h\nu$ = 258 cm^{-1}; A_1 = 940 cm^{-1}; and d_x, d_y, d_z, and d_o are the Zn−O(8), Zn−O(7), Zn−O(9), and average Zn−O bond lengths, respectively. A negative sign for S_θ indicates that the tetragonal strain acts as a compression, a common feature of the Tutton's salts due to the M−O(9) distance being the shortest bond length, irrespective of the transition metal or counterions. Accordingly, with a negative value for S_θ, a positive value of S_ε corresponds to a relative stabilization of the JT minimum in the second quadrant ($-Q_\theta$, $+Q_\varepsilon$) at ϕ = ∼120°, which in turn corresponds to a relative elongation of the bonds along the x direction, and a negative value of S_ε corresponds to a relative stabilization in the third quadrant ($-Q_\theta$, $-Q_\varepsilon$) at ϕ = ∼240° with a relative elongation of the bonds along the y direction.

The values of S_θ obtained from eq 3 and the Zn−O bond lengths given in Table 1 give ∼−1100 and −1300 cm^{-1} for the Rb^+ and K^+ compounds, respectively, significantly higher than our best-fit values in Table 4 (−530 and −650 cm^{-1}). The values for S_ε calculated from eq 4 give ∼60 and −80 cm^{-1} for the Rb^+ and K^+ compounds, respectively, much lower than the best fit values of 287 and −385 cm^{-1} from experimental data (Table 4). While the signs of the basic distortions of the pure copper(II) Rb^+ and K^+ compounds are correctly predicted from eqs 3 and 4 and the structures of the isomorphous zinc

Table 4. Optimum Potential Energy Surface Parameters for $K_{2x}Rb_{2-2x}[Cu(H_2O)_6](SeO_4)_2$ Complexes, See Text

	$h\nu_{JT}$ (cm^{-1})	A_1 (cm^{-1})	A_2/β (cm^{-1})	S_θ (cm^{-1})	S_ε (cm^{-1})
$Rb_2[Cu(H_2O)_6](SeO_4)_2$, x = 0	258	940	13/173	−530	287
x = 0.127	258	940	13/173	−505	250
x = 0.262	258	940	13/173	−500	230
x = 0.318	258	940	13/173	−500	200
x = 0.359	258	940	13/173	−490	210
x = 0.390	258	940	13/173	−520	215[a]
x = 0.411	258	940	13/173	−520	215[a]
x = 0.498	258	940	13/173	−500	−205
x = 0.728	258	940	13/173	−590	−290
$K_2[Cu(H_2O)_6](SeO_4)_2$, x = 1.0	258	940	13/173	−650	−385

[a]Values of S_ε determined in low-temperature region 90−170 K; S_ε ∼ −100 cm^{-1} for x = 0.411 at 298 K.

dx.doi.org/10.1021/ic401385f | Inorg. Chem. 2013, 52, 10481−10499

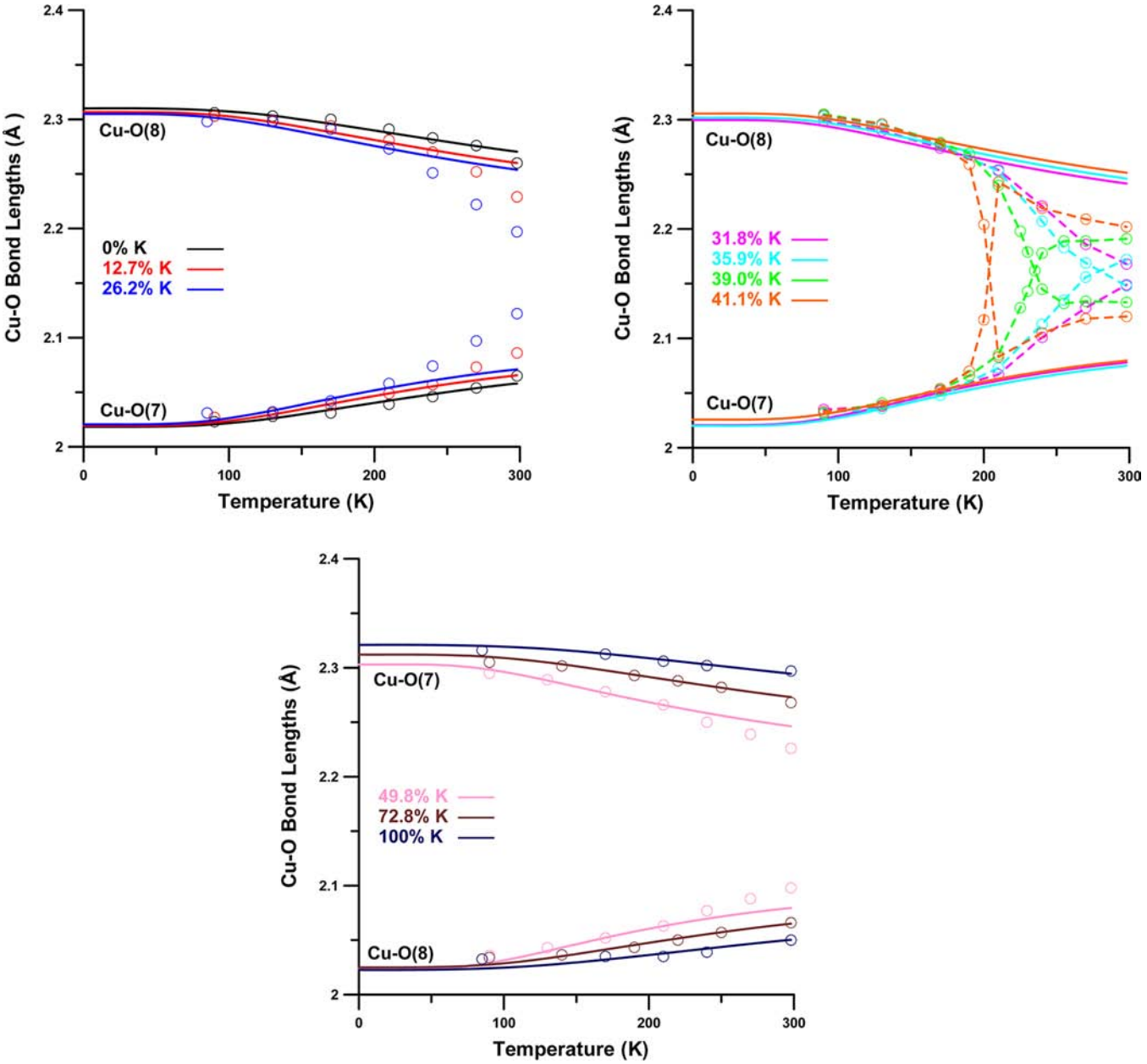

Figure 7. Plots of Cu−O bond lengths calculated using the RHW model with the best-fit parameters given in Table 4 (solid curves) and experimental bond lengths given in Table 1 (open circles) for $K_{2x}Rb_{2-2x}[Cu(H_2O)_6](SeO_4)_2$ crystals with 0, 12.7, and 26.2% K^+ (left); 31.8, 35.9, 39.0, and 41.1% K^+ (right); and 49.8, 72.8, and 100% K^+ (bottom) as a function of temperature. Experimental bond lengths can be fitted very accurately to ∼170 K using the RHW model; however, deviations occur above that temperature as a result of cooperative JT interactions, the magnitude of which depends on the K^+ dopage and temperature.

compounds, the magnitudes are not. Better agreement for estimating S_θ and S_ε, however, is found using eqs 3 and 4 and the zinc structures when compared to experiments on the doped zinc compounds. For example, fitting the EPR data for the $[Cu(H_2O)_6]^{2+}$ ion doped into the sulfate host lattices $X_2[Zn(H_2O)_6](SO_4)_2$ gives S_θ ranging from −1000 to −550 cm^{-1} and S_ε from 55 to 200 cm^{-1} along the series X = K^+, Rb^+, Cs^+, and NH_4^+.[42] However, it is clear that provided the warping of the potential energy surface is relatively large, as it is in the case for the $[Cu(H_2O)_6]^{2+}$ ion, it follows that the temperature dependence of the long and intermediate Cu−O bond lengths depends mainly upon the energy difference between the two lower minima in the potential surface, i.e., the orthorhombic component of the strain, S_ε, while the short Cu−O(9) bond length is decided largely by S_θ.

It is interesting to consider a possible relationship between the orthorhombic strain values determined using the RHW model in the absence of cooperative JT interactions, S_ε, and those expressed by Δ based on $O_{donor}\cdots O_{acceptor}$ contact distances developed earlier. Accordingly, Figure 8 shows that S_ε, starting with pure $Rb_2[Cu(H_2O)_6](SeO_4)_2$ (form **A**), has a positive value which decreases linearly to a 41.1% K^+ dopage, after which it drops precipitously to zero at ∼45% K^+ and then becomes progressively more negative from 49.8 to 100% K^+ for form **B** complexes. The fact that both S_ε and Δ appear to be linear functions of the K^+-dopage allows us to write the

dx.doi.org/10.1021/ic401385f | *Inorg. Chem.* 2013, 52, 10481−10499

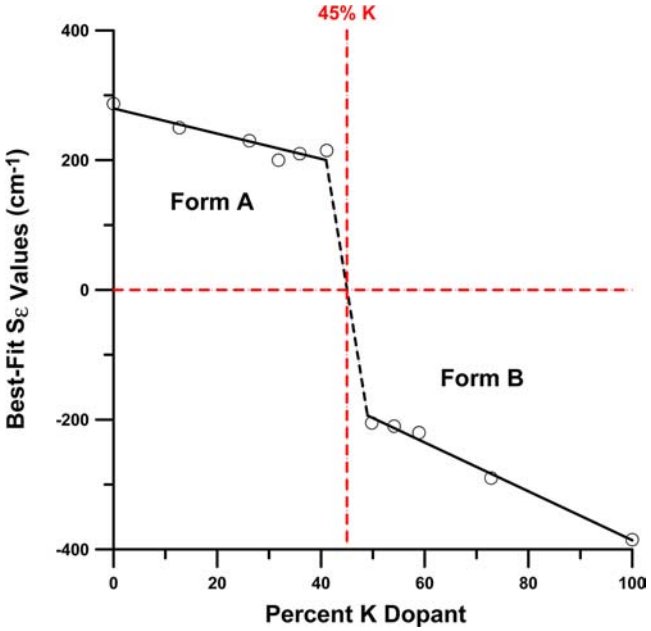

Figure 8. Linear least-squares fits of the orthorhombic best-fit strain parameters in the absence of cooperative JT interactions, S_ε, vs %K^+ dopant concentration for mixed $K_{2x}Rb_{2-2x}[Cu(H_2O)_6](SeO_4)_2$ crystals. At ~45% K^+, the orthorhombic strain is predicted to be zero.

following equations relating them for form **A** and **B** complexes, respectively, within prescribed limits

$$S_\varepsilon\ (\mathrm{cm}^{-1}) = 280 - 5000[\Delta\ (\text{Å}) - 0.070] \qquad 0.070 < \underset{\text{form A}}{\Delta\ (\text{Å})} < 0.086 \tag{5a}$$

and

$$S_\varepsilon\ (\mathrm{cm}^{-1}) = -193 - 9650[\Delta\ (\text{Å}) - 0.089] \qquad 0.089 < \underset{\text{form B}}{\Delta\ (\text{Å})} < 0.109 \tag{5b}$$

A more reliable way to check the accuracy and consistency of our best-fit parameters is with the following equation, which relates the energy of the optical transition between the tetragonally split components of the ^2E_g (O_h) ground term of the $[Cu(H_2O)_6]^{2+}$ ion, $\Delta(^2E_g)$, to the corresponding values of $h\nu_{JT}$, A_1 and S_θ, ignoring orthorhombic strain and higher-order vibronic coupling[42]

$$\Delta(^2E_g) = (2A_1^{\,2}/h\nu_{JT}) + 2|S_\theta| \tag{6}$$

Using the values of the parameters for the pure Rb^+ and K^+ complexes given in Table 4, the values of $\Delta(^2E_g)$ obtained using this equation are 7910 and 8150 cm^{-1}. It should be noted that Dobe et al.[39] measured a value of ~8000 cm^{-1} for the $\Delta(^5E_g)$

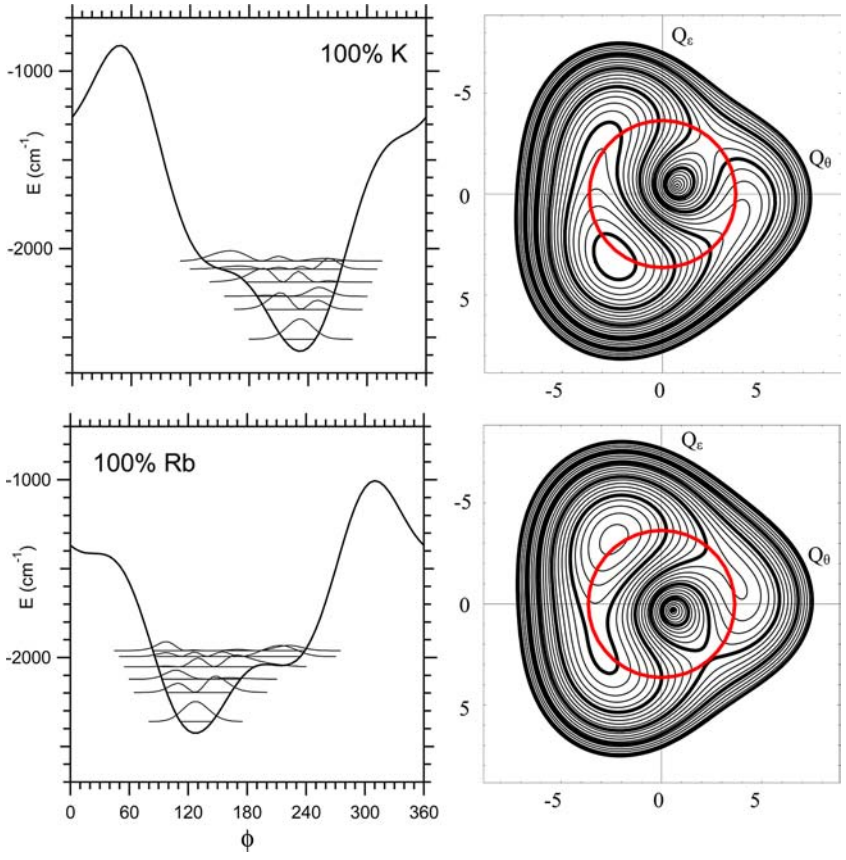

Figure 9. The potential surface of the $[Cu(H_2O)_6]^{2+}$ ion in pure $K_2[Cu(H_2O)_6](SeO_4)_2$ and $Rb_2[Cu(H_2O)_6](SeO_4)_2$ plotted as a function of the JT e_g coordinates (Q_θ, Q_ε) (right) and as a function of ϕ at a fixed value of $\rho_o = A_1/h\nu$ (left). The potentials have been calculated with eq 2 and the parameters given in Table 4. The contour lines are drawn every 100 cm^{-1}, with every 500 cm^{-1} in bold. The circle at constant ρ_o shows the cross-section of the one-dimensional plots on the left. The energy of the six lowest vibronic levels are shown on the one-dimensional surface, where a zero point energy of $1/2h\nu$ is subtracted to account for removing the ρ dimension. The squares of the vibrational components of the six lowest vibronic wave functions are also shown.

dx.doi.org/10.1021/ic401385f | Inorg. Chem. 2013, 52, 10481−10499

transition from the spectrum of the JT $(NH_4)_2[Cr(H_2O)_6](SO_4)_2$ complex at 13 K, whereas Hitchman and Waite[58] observed $\Delta(^2E_g)$ values of ~7800 and 8150 cm^{-1} for $Rb_2[Cu(H_2O)_6](SO_4)_2$ (95 K) and $K_2[Cu(D_2O)_6](SO_4)_2$ (95 K), respectively. Because of the close agreement between the calculated and observed $\Delta(E_g)$ values, our assumed $h\nu_{JT}$ value and best-fit A_1 and S_θ values appear to be quite reasonable.

The RHW model calculates Cu−O bond lengths and energies associated with each vibronic level; these are then used to calculate the overall Boltzmann weighted average Cu−O bond lengths per the following equations[20]

$$d(\mathrm{Cu-O})_{calc} = \Sigma_i Z \exp(-\varepsilon_i/kT)\langle d(\mathrm{Cu-O})\rangle_i \text{ and } Z = [\Sigma_i \exp(-\varepsilon_i/kT)]^{-1} \quad (7)$$

where $\langle d(Cu-O)\rangle_i$ are the calculated Cu−O bond lengths associated with vibronic level i with energy ε_i. We consider that the systematic deviations between calculated and observed Cu−O bond lengths are most likely a result of cooperative JT interactions, which are associated with deviations from the Boltzmann weighted average given by eq 7 above. Accordingly, the fits in Figure 7 show excellent agreement for the pure Rb^+ and K^+ complexes, although it should be noted that their corresponding S_ε values, 287 and −385 cm^{-1}, respectively, are relatively large, and only at high temperatures should the effects of cooperative JT interactions become discernible, as is indicated by the slight negative deviations exhibited for the Rb^+ complex at room temperature. For the mixed K^+/Rb^+ complexes, deviations increase as the amount of K^+ dopant (added to form **A** complexes) or Rb^+ dopant (added to form **B** complexes) increases at a given temperature, which was also observed in the analogous $K_2[Cu(H_2O)_6](SO_4)_{2-2x}(SeO_4)_{2x}$ mixed complexes.[20] Nonetheless, a close inspection of the plots reveals that even for the 35.9, 39.0, and 41.1% K^+ complexes, which exhibit extreme temperature dependence in Cu−O bond lengths, optimum agreement with the experimental data is achieved to at least ~170 K, after which substantial deviations occur. The interpretation of the X-ray data shown in Figure 5 (left) that cooperative JT interactions in $K_{2x}Rb_{2-2x}[Cu(H_2O)_6](SeO_4)_2$ crystals are essentially negligible until at ~170 K is in complete agreement with the results obtained using the RHW model as shown in Figure 7.

The JT radius, R_{JT}, of the $[Cu(H_2O)_6]^{2+}$ ion, defined as $R_{JT} = [2(d_x)^2 + 2(d_y)^2 + 2(d_z)^2]^{1/2}$, where d_x, d_y, and d_z are the differences in bond lengths along each bond direction from the mean value, is slightly different for the two forms: R_{JT} = 0.390 and 0.378 Å for the pure potassium (form **B**) and pure rubidium (form **A**) salts at 85 and 90 K, respectively. This represents a marked difference from $(NH_4)_2[Cu(H_2O)_6](SO_4)_2$ and its deuterated analogue. Here, the deuterated salt in form **A** has a slightly larger distortion than the hydrogenous compound in form **B**: R_{JT} = 0.37 and 0.34 Å, respectively, although it is unclear how this is related to the relative stability of the two forms.[7,10,59]

Contour plots of the lower adiabatic potential energy surfaces of the $[Cu(H_2O)_6]^{2+}$ ion in the crystal lattices of the pure potassium and rubidium compounds as calculated using eq 2 and the optimum values given Table 4 are shown in Figure 9. Also shown are energy plots at the circular cross sections at the JT radius ρ_o indicated, along with the first six vibronic energy levels and their probability functions. The most striking feature is the fact that with these parameters there are not three distinct minima at values of $\phi \sim 0$, 120, and 240° as would occur in the absence of the low symmetry strain terms, but rather a single minimum with two additional very shallow minima or shoulders in the energy surface. The energy minimum occurs close to 120° when the compound adopts form **A** (Rb^+) and 240° when it is in form **B** (K^+). These angles correspond to tetragonal elongations with the long axes along x and y, respectively. (Note that the direction of the axial strain, which is associated with the shortest Cu−O bond, is defined as the z axis.[42,54]) The bond lengths associated with the six lowest vibronic states of each potential surface are given in Table 5.

Table 5. Calculated Energy and Geometry for the First Six Vibronic Levels for the Pure Compounds Using the Parameters Given in Table 4

level	energy (cm^{-1})	R_x (Å)	R_y (Å)	R_z (Å)
$Rb_2[Cu(H_2O)_6](SeO_4)_2$				
1	0.0	2.3101	2.0184	1.9463
2	164.0	2.2959	2.0367	1.9421
3	239.3	2.3062	2.0192	1.9439
4	308.3	2.2530	2.0923	1.9294
5	366.7	2.1876	2.1546	1.9325
6	399.6	2.2459	2.0826	1.9462
$K_2[Cu(H_2O)_6](SeO_4)_2$				
1	0.0	2.0227	2.3210	1.9421
2	167.7	2.0389	2.3084	1.9384
3	241.8	2.0217	2.3190	1.9451
4	322.0	2.0705	2.2849	1.9303
5	395.1	2.0547	2.2898	1.9412
6	440.3	2.1250	2.2338	1.9269

The calculated overall bond lengths are compared with those observed experimentally for each compound as a function of temperature in Figure 7. It should be noted that the axial strain is the dominant factor influencing the energy of the highest of the three mimina/shoulders in the potential surface at $\phi \sim 0°$ corresponding to an elongation along z. Because $|S_\theta|$ is large, the energy difference between highest and lowest energy minima is substantial, ~1100 cm^{-1}, which means that the Cu−O(9) bond lengths do not vary with temperature up to at least 300 K.

Note that with these parameter values and the lack of more than one distinct minimum on the potential energy surface as shown in Figure 9, one does not have a simple classical picture of a higher energy level localized at a minimum that has a different geometry to that of the lowest energy minimum. Rather, there is a single asymmetric minimum that is shallow in one direction. At low temperatures, the $[Cu(H_2O)_6]^{2+}$ complexes are in their lowest vibronic level, which as shown in Figure 9, has its probability function localized at the minimum. As the temperature is raised, higher vibronic levels are populated that are more delocalized, particularly in the direction for where the potential is the shallowest. Conceptionally, this picture is quite different: instead of populating a higher level at a different geometry (bonds along x and y axes switched), one is populating higher levels that do not have a distinct geometry but are more delocalized. Computationally, there is no difference, the expectation values of the coordinates can be calculated for each level, and their thermal populations can be determined using the energy of each level.[20,42]

For both the pure potassium and rubidium salts, the second-lowest minimum of the potential surface is not clearly defined (Figure 9), and the vibronic wave functions above the lowest

dx.doi.org/10.1021/ic401385f | Inorg. Chem. 2013, 52, 10481−10499

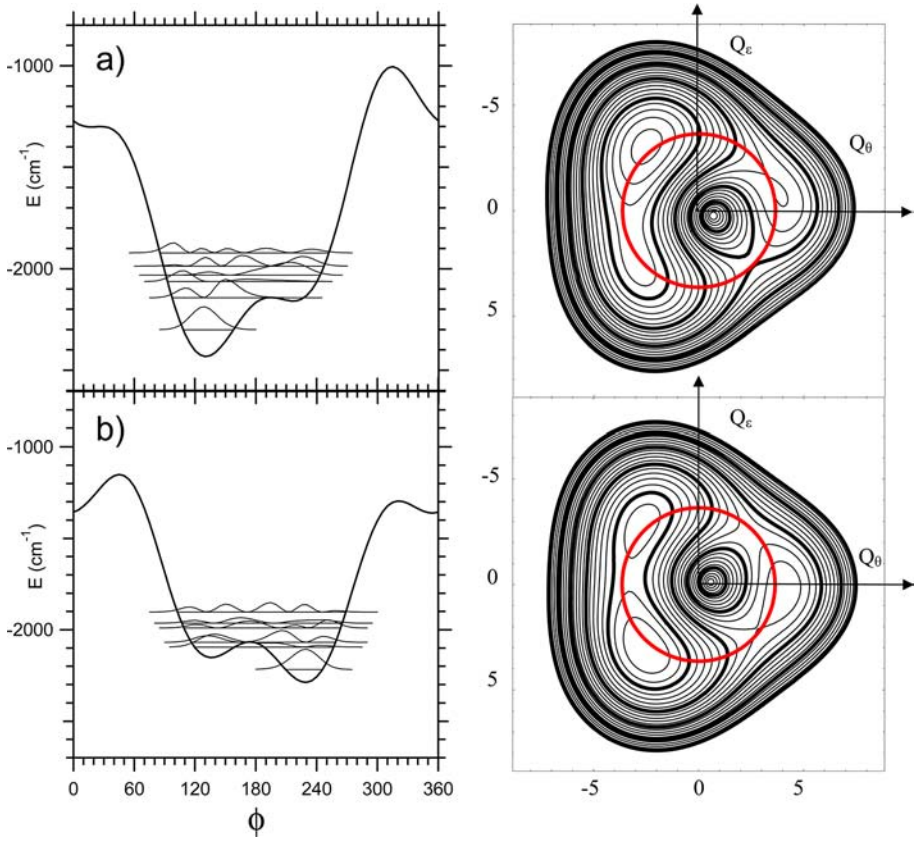

Figure 10. The potential surface of the $[Cu(H_2O)_6]^{2+}$ ion in $K_{2x}Rb_{2-2x}[Cu(H_2O)_6](SeO_4)_2$ for 41.1% K^+ plotted as a function of the JT e_g coordinates (Q_θ, Q_ε) (right) and as a function of ϕ at a fixed value of $\rho_o = A_1/h\nu$ (left). The potentials have been calculated from fitting the data in various temperature ranges and have the parameters: A_1 = 940 cm^{-1}, A_2 = 13 cm^{-1}, S_θ = −520 cm^{-1}, and S_ε the following values: (a) T = 90−170 K, S_ε = 215 cm^{-1}; and (b) T = 220−298 K, S_ε = −100 cm^{-1}; see the caption to Figure 9 for more details.

energy level are quite delocalized (Table 5). For these complexes, there is no single energy level corresponding to a tetragonally elongated geometry with the direction of the long axis switched compared with that of the lowest level. Instead, levels with bonds along x and y approximately equal in length occur (levels 5 and 6 for the Rb^+ and K^+ compounds, respectively). This situation has been observed for other compounds[42,51,55] and occurs when the orthorhombic component of the strain is comparable in magnitude to the warping parameter β. Although thermal occupancy of these upper levels has a similar effect on the population of a single level with the bond lengths along x and y interchanged, these compounds formally deviate from this simplistic assumption.

For the mixed $K_{2x}Rb_{2-2x}[Cu(H_2O)_6](SeO_4)_2$ crystals with 0 < %K^+ < 31 and 49 < %K^+ < 100, the observed Cu−O(7) and Cu−O(8) bond lengths gradually converge as the temperature is raised from 90 to 300 K (Figure 3); similar behavior has been observed for many other complexes, both by X-ray diffraction[15,60] and EPR spectroscopy.[42,52,55] As discussed previously, this aspect may be interpreted satisfactorily in terms of a thermal equilibrium between the vibronic wave functions of a potential surface which does not change significantly with temperature. This is only an approximation, because the potential surface may change slightly if the strain induced by the lattice varies with temperature,[55] or if cooperative interactions are present.[11,20] However, for the salts having between 32 < %K^+ < 41, an additional much more rapid change in the Cu−O distances occurs, with the directions of the long and intermediate bonds interchanging. For example, the salt with 41.1% K^+ adopts the crystal structure of form **A** between 90 and ∼170 K (Figure 3), and the potential surface of the $[Cu(H_2O)_6]^{2+}$ ion is as shown in Figure 10a, with the Cu−O bond lengths depending on the thermal population of the vibronic wave functions. Between ∼220 and ∼300 K, the crystal structure switches to that of form **B**, and the Cu−O bond lengths are determined by a thermal population of the vibronic functions of the potential surface shown in Figure 10b. This interpretation implies that when the crystal structure suggests that the Cu−O bond lengths are equal at 205 K (Figure 3), this does not mean that every complex is identical, with two minima equal in energy, as has been inferred for some other compounds showing tetragonal symmetry of the bond lengths.[61,62] Rather, the crystal contains an equal proportion of unit cells of form **A** with potential surfaces as shown in Figure 10a and of form **B** with potential surfaces shown in Figure 10b.

Analysis of Experimental Values for ΔU_{obs}. Disorder resulting from the thermal equilbrium between complexes of different forms in $K_{2x}Rb_{2-2x}[Cu(H_2O)_6](SeO_4)_2$ crystals can be analyzed in terms of differences in mean-square displacement amplitudes along Cu−O bonds, ΔU_{obs}(Cu−O) (Å^2), which are listed in Table 1. ΔU values between pairs of atoms are a way of quantifying JT distortions when taken between the metal and ligand atoms along the direction of the metal−ligand bond. The observed quantity, ΔU_{obs}, will be the sum of the usual small amplitude atomic displacement due to bond stretching motions, $\langle \Delta U_{stretch} \rangle$, and to the large amplitude JT distortion, ΔU_{dis}

dx.doi.org/10.1021/ic401385f | Inorg. Chem. 2013, 52, 10481−10499

$$\Delta U_{obs} = \langle \Delta U_{stretch} \rangle + \Delta U_{dis} \quad (8)$$

Stebler and Bürgi[63] have, in effect, shown how the ΔU_{obs}'s can be calculated for a copper(II) JT complex such as the $[Cu(H_2O)_6]^{2+}$ ion in mixed crystals of $K_{2x}Rb_{2-2x}[Cu(H_2O)_6](SeO_4)_2$ that essentially obeys the Silver and Getz model. Accordingly, the temperature variation of the observed Cu−O(7) and Cu−O(8) bond lengths is assumed to be the result of the thermal equilibrium between two JT-structural isomers (each associated with an energy minimum labeled with a subscript 1 or 2) differing solely by the interchange of the directions of the long (l) and intermediate (i) bonds, i.e., $d[Cu{-}O(7)^l]_1 = d[Cu{-}O(8)^l]_2$ and $d[Cu{-}O(8)^i]_1 = d[Cu{-}O(7)^i]_2$. Equation 8 can be rewritten as[63]

$$\Delta U_{obs} = a_o + a_1\langle \Delta d(Cu-O)\rangle - \langle \Delta d(Cu-O)\rangle^2 \quad (9)$$

where the temperature-independent coefficients a_o and a_1 are $a_o = (\Delta U_l + \Delta U_i)/2 + [\Delta d(Cu{-}O)]^2$ and $a_1 = (\Delta U_l - \Delta U_i)/2\Delta d(Cu{-}O)$; ΔU_1 and ΔU_i are contributions from internal stretching motions unrelated to JT distortion. Also, $\Delta d(Cu{-}O) \equiv \{d[Cu{-}O(7)^l]_l - d[Cu{-}O(7)^i]_2\}_{static}/2 = \{d[Cu{-}O(8)^l]_2 - d[Cu{-}O(8)^i]_1\}_{static}/2 = \{d[Cu{-}O(7)^l]_1 - d[Cu{-}O(8)^i]_1\}_{static}/2 = \{d[Cu{-}O(8)^l]_2 - d[Cu{-}O(7)^i]_2\}_{static}/2$, or half the difference in the long and intermediate static bond lengths of each complex, and $\langle \Delta d(Cu{-}O)\rangle \equiv \{\langle d[Cu{-}O(8)]\rangle - \langle d[Cu{-}O(7)]\rangle\}/2$, or half the difference in the observed, nonstatic bond lengths. This equation predicts that there will be a quadratic dependence of the ΔU_{obs} values on half the difference in the observed bond lengths, $\langle \Delta d(Cu{-}O)\rangle$, that $\Delta U_{obs}(max) = a_o + a_1^2/4 \sim a_o$ at $\langle \Delta d(Cu{-}O)\rangle = a_1/2 \sim 0$. Therefore, according to this model, $\Delta U_{obs}(max)$ occurs when the observed Cu−O(7) and Cu−O(8) bond lengths are equal, i.e., at the transition temperature between forms **A** and **B**.

The anisotropic displacement parameters allow ΔU_{obs} values to be calculated, which are given in Table 1 for each structure at different temperatures. Generally, the values of $\Delta U_{obs}[Cu{-}O(7)]$ and $\Delta U_{obs}[Cu{-}O(8)]$ are nearly equal and show a marked temperature dependence, rising significantly with increasing temperature; in addition, they show discernible maxima at the transition temperatures for those mixed complexes with 32 < K% < 41. For example, for 39% K^+ at T = 235 K, Cu−O(7) = Cu−O(8) = 2.162(2) Å and $\Delta U_{obs}[Cu{-}O(7)] = 0.021(1)$ Å^2 and $\Delta U_{obs}[Cu{-}O(8)] = 0.020(1)$ Å^2, which agree exactly with the maximum ΔU_{obs} value calculated using the Stebler−Bürgi model (0.021 Å^2; *vide infra*). In contrast, the values of $\Delta U_{obs}[Cu{-}O(9)]$ are much smaller (except at very low temperatures) and are nearly constant with temperature, as reflected by the fact that the energy minimum associated with the short Cu−O(9) bond at $\phi \sim 0°$ lies at a substantially higher energy (~1100 cm^{-1}) than the two minima involved in the thermal equilibrium located at ~120 and 240°.

The Stebler−Bürgi scatter-plot of ΔU_{obs} vs $\langle \Delta d(Cu{-}O)\rangle$ is shown in Figure 11. A structure determination at a given temperature contributes two points: $\Delta U_{obs}[Cu{-}(O7)]$ at negative $\langle \Delta d(Cu{-}O)\rangle$ and $\Delta U_{obs}[Cu{-}O(8)]$ at positive $\langle \Delta d(Cu{-}O)\rangle$; the coefficients of the quadratic term have been constrained to be −1 to conform with eq 9. In general there is very good agreement with the predicted quadratic dependence of eq 9. Since $a_o = 0.0210$ Å^2 and $a_1 = 0.0026$ Å, $\Delta U_{obs}(max) \sim 0.0210$ Å^2, which is essentially identical to the values of 0.0214 and 0.022 Å^2 reported for a study of $(ND_4)_2[Cu(D_2O)_6](SO_4)_2$ and $(NH_4)_2[Cu(H_2O)_6](SO_4)_2$[38]

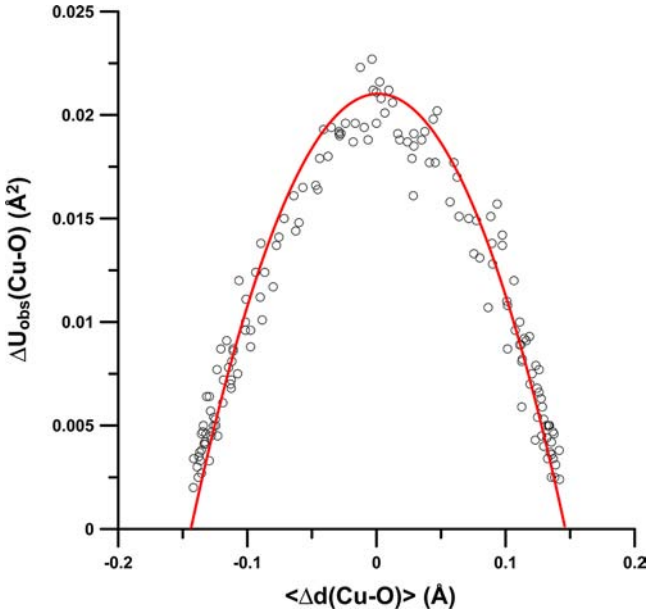

Figure 11. Stebler−Bürgi scatter plot of $\Delta U_{obs}(Cu{-}O)$ (Å^2) vs $\langle \Delta d(Cu{-}O)\rangle$ (Å) for mixed crystals of $K_{2x}Rb_{2-2x}[Cu(H_2O)_6](SeO_4)_2$ with 0, 12.7, 26.2, 31.8, 35.9, 39.0, 41.1, 49.8, 72.8, and 100% K^+. The solid red line represents the best-fit quadratic eq 9: $\Delta U_{obs}(Cu{-}O) = a_o + a_1\langle \Delta d(Cu{-}O)\rangle - \langle \Delta d(Cu{-}O)\rangle^2$, where $a_o = 0.0210$ Å^2 and $a_1 = 0.0026$ Å; 156 points, $R^2 = 0.940$; see text.

and $K_2[Cu(H_2O)_6](SO_4)_{2-2x}(SeO_4)_{2x}$,[20] respectively. Furthermore, we can estimate the value of $\Delta U_l + \Delta U_i$ in eq 9 from the $\Delta U_{obs}(Zn{-}O)$ values given in Table 1 for the non-JT Tutton's salts, $Rb_2[Zn(H_2O)_6](SeO_4)_2$ and $K_2[Zn(H_2O)_6](SeO_4)_2$, as 0.0030−0.0040 Å^2, which, knowing the value of a_o (0.0210 Å^2), allows us to calculate the value of $2\Delta d(Cu{-}O) = l\{d[Cu{-}O(8)] - d[Cu{-}O(7)]\}l_{static}$ as 0.276−0.279 Å. An inspection of the Cu−O(7) and Cu−O(8) static bond lengths observed for various copper(II) Tutton's salts given in Table 6 indicates excellent agreement.

CONCLUSIONS

In the mixed-cation series $K_{2x}Rb_{2-2x}[Cu(H_2O)_6](SeO_4)_2$, the long and intermediate bonds of the JT distorted $[Cu(H_2O)]_6^{2+}$ ion occur to different water molecules in the regions ~0−31% (form **A**) and ~49−100% K^+ (form **B**). The coordination number of the alkali metal differs in the two crystal forms, being eight in form **A** and seven in form **B**. This difference in coordination number is associated with a partial rotation of a selenate group which is hydrogen-bonded to a water molecule involved in the switching of the JT distortion of the $[Cu(H_2O)]_6^{2+}$ ion. Between ~32 and ~45% potassium, the crystal structure changes relatively sharply from form **A** to form **B** on warming from 90 to 300 K, with the temperature at which this occurs falling approximately linearly as the proportion of potassium increases. The Cu−O bond lengths show an additional, gradual convergence on warming, and this is interpreted quantitatively in terms of a thermal equilibrium between the vibronic energy levels of the JT potential surface of the $[Cu(H_2O)_6]^{2+}$ ion under the influence of a lattice strain used to quantify the low site symmetry. The orthorhombic component of the lattice strain decreases in magnitude as the proportion of potassium becomes more nearly equal to that of rubidium and changes sign when the compound switches from form **A** to form **B**. It is this change in sign of the lattice strain

dx.doi.org/10.1021/ic401385f | *Inorg. Chem.* 2013, 52, 10481−10499

Table 6. Static d[Cu−O(7)] and d[Cu−O(8)] Bond Lengths for Copper(II) Tutton's Salts

complex	T (K)	d[Cu−O(7)] Å	d[Cu−O(8)] Å	2Δd(Cu−O) Å	ref
$K_2[Cu(H_2O)_6](SO_4)_2$[c]	15	2.034(2)	2.316(1)	0.282	7a
$(NH_4)_2[Cu(H_2O)_6](SO_4)_2$[c]	14	2.272(2)	2.005(2)	0.267	4
$(NH_4)_2[Cu(H_2O)_6](SO_4)_2$	9.5	2.2758(9)	2.0042(8)	0.272	59
$(NH_4)_2[Cu(H_2{}^{18}O)_6](SO_4)_2$	9.5	2.2769(9)	2.0019(8)	0.275	59
$(NH_4)_2[Cu(H_2O)_6](SO_4)_2$	15	2.2834(5)	2.0077(5)	0.276	10
$(ND_4)_2[Cu(D_2O)_6](SO_4)_2$	5	2.011(4)	2.304(6)	0.293	2
$(ND_4)_2[Cu(D_2O)_6](SO_4)_2$	15	2.007(21)	2.298(7)	0.291	*a*
$(ND_4)_2[Cu(D_2O)_6](SO_4)_2$	9	2.0093(4)	2.3002(5)	0.291	*b*
$(ND_4)_2[Cu(D_2O)_6](SO_4)_2$	15	2.022(2)	2.310(2)	0.288	4
$(ND_4)_2[Cu(D_2O)_6](SO_4)_2$[d]	15	2.290(2)	2.014(2)	0.276	4
$(ND_4)_2[Cu(D_2O)_6](SO_4)_2$[e]	15	2.2802(4)	2.0082(4)	0.272	10

[a]Iversen, B. B.; Larsern, F. K.; Reynolds, P. A.; Figgis, B. N. *Acta Chem. Scand.* **1994**, *48*, 800−809. [b]Figgis, B. N.; Iversen, B. B.; Larsen, F. K.; Reynolds, P. A. *Acta Crystallogr.* **1993**, *B49*, 794−806. [c]Pressure = 1.4 kbar. [d]Pressure = 1.5 kbar. [e]Prepared in metastable state.

which causes the long axis of the JT distortion to switch direction between the crystal forms.

■ ASSOCIATED CONTENT

Supporting Information

X-ray crystallographic data in CIF format for 78 structure determinations of $K_{2x}Rb_{2-2x}[Cu(H_2O)_6](SeO_4)_2$ and two for $K_2[Zn(H_2O)_6](SeO_4)_2$ and $Rb_2[Zn(H_2O)_6](SeO_4)_2$; X···O distances (Å) in XO_n^+ polyhedra for $X_2[M(H_2O)_6](SeO_4)_2$ and $X_2[M(H_2O)_6](SO_4)_2$ Tutton's salts (S1A and S1B); Δ (Å) values for non-JT selenate and sulfate salts (S2A and S2B); two-dimensional plots of wave functions for vibronic levels for $K_2[Cu(H_2O)_6](SeO_4)_2$ (S3); and 22 pages (Tables SA−SK) of X-ray crystallographic data and structural refinements. This material is available free of charge via the Internet at http://pubs.acs.org.

■ AUTHOR INFORMATION

Corresponding Author

*E-mail: simmonsc@hawaii.edu.

Notes

The authors declare no competing financial interest.

■ REFERENCES

(1) Named after Alfred Edwin Howard Tutton (1861−1938), an English mineralogist. Several Tutton's salts are found as naturally occurring minerals, viz., picromerite $K_2[Mg(H_2O)_6](SO_4)_2$, cyanochroite $K_2[Cu(H_2O)_6](SO_4)_2$, boussingaultite $(NH_4)_2[Mg(H_2O)_6](SO_4)_2$, nickel-boussingaultite $(NH_4)_2[Ni(H_2O)_6](SO_4)_2$, and mohrite $(NH_4)_2[Fe(H_2O)_6](SO_4)_2$: Bosi, F.; Belardi, G.; Ballirano, P. *Am. Mineral.* **2009**, *94*, 74−82.

(2) Hathaway, B. J.; Hewat, A. W. *J. Solid State Chem.* **1984**, *51*, 364−375.

(3) Montgomery, H.; Lingafelter, E. *Acta Crystallogr.* **1966**, *20*, 659−662.

(4) Simmons, C. J.; Hitchman, M. A.; Stratemeier, H.; Schutz, A. J. *J. Am. Chem. Soc.* **1993**, *115*, 11304−11311.

(5) Chen, Z.; Fei, S.; Strauss, H. L. *J. Am. Chem. Soc.* **1998**, *120*, 8789−8796.

(6) Simmons, C. J.; Hitchman, M. A.; Stratemeier, H.; Astley, T. *Inorg. Chem.* **2000**, *39*, 4651−4653.

(7) (a) Rauw, W.; Ahsbahs, H.; Hitchman, M. A.; Lukin, S.; Reinen, D.; Schultz, A. J.; Simmons, C. J.; Stratemeier, H. *Inorg. Chem.* **1996**, *35*, 1902−1911. (b) Schultz, A. J.; Hitchman, M. A.; Jorgensen, J. D.; Lukin, S.; Radaelli, P. G.; Simmons, C. J.; Stratemeier, H. *Inorg. Chem.* **1997**, *36*, 3382−3385.

(8) Schultz, A. J.; Henning, R. W.; Hitchman, M. A.; Stratemeier, H. *Cryst. Growth Des.* **2003**, *3*, 403−407.

(9) Augustyniak, M. A.; Krupski, M. *Chem. Phys. Lett.* **1999**, *311*, 126−130.

(10) Dobe, C.; Carver, G.; Bürgi, H.-B.; Treggenna-Piggott, P. L. W.; McIntyre, G. J.; Augustyniak-Jablokow, M. A.; Riley, M. J. *Inorg. Chem.* **2003**, *42*, 8524−8533.

(11) Hitchman, M. A.; Maaskant, W.; van der Plas, J.; Simmons, C. J.; Stratemeier, H. *J. Am. Chem. Soc.* **1999**, *121*, 1488−1501.

(12) (a) Figgis, B. N.; Kucharski, E. S.; Reynolds, P. A. *Acta Crystallogr.* **1990**, *B46*, 577−586. (b) Figgis, B. N.; Kucharski, E. S.; Forsyth, J. B. *Acta Crystallogr.* **1991**, *C47*, 419−421.

(13) Dobe, C.; Strassle, T.; Juranyi, F.; Tregenna-Piggott, P. L. W. *Inorg. Chem.* **2006**, *45*, 5066−5072.

(14) (a) Araya, M. A.; Cotton, F. A.; Daniels, L. M.; Falvello, L. R.; Murillo, C. A. *Inorg. Chem.* **1993**, *32*, 4853−4860. (b) Cotton, F. A.; Daniels, L. M.; Falvello, L. R.; Murillo, C. A.; Schultz, A. J. *Inorg. Chem.* **1994**, *33*, 5396−5403.

(15) (a) Hitchman, M. A. *Comments Inorg. Chem.* **1994**, *15*, 197−254. (b) Falvello, L. R. *J. Chem. Soc., Dalton Trans.* **1997**, 4463−4475.

(16) Augustyniak, M. A.; Usachev, A. E. *J. Phys.: Condens. Matter* **1999**, *11*, 4391−4400.

(17) Henning, R. W.; Schultz, A. J.; Hitchman, M. A.; Kelly, G.; Astley, T. *Inorg. Chem.* **2000**, *39*, 765−769.

(18) Fleck, M.; Kolitsch, U. *Z. Kristallogr.* **2002**, *217*, 15−16.

(19) Whitnall, J.; Kennard, C. H. L.; Nimmo, J. K.; Moore, F. H. *Cryst. Struct. Commun.* **1975**, *4*, 709−712.

(20) Simmons, C.J..; Stratemeier, H.; Hitchman, M. A.; Riley, M. J. *Inorg. Chem.* **2006**, *45*, 1021−1031.

(21) Simmons, C. J.; Stratemeier, H.; Hitchman, M. A. Unpublished results.

(22) Otwinowski, Z.; Minor, W. *Methods Enzymol.*; Carter, C. W., Jr., Sweet, R. M., Eds.; Academic Press: New York, 1997; Vol. *276*, 307−326.

(23) It should be noted that it was possible for the K^+/Rb^+ mixed crystals to split the selenate O atoms into two groups and refine each group separately (with a common, unsplit central Se atom) with approximately the same occupancies as the K^+ and Rb^+ cations. The starting positional parameters for one group were taken from the structure of pure $K_2[Cu(H_2O)_6](SeO_4)_2$,[19,20] the other from pure $Rb_2[Cu(H_2O)_6](SeO_4)_2$.[18] The R and goodness of fit values decreased only slightly for the split model. For example, for 49.8% K^+ at T = 298 K, the unsplit model gave R_1 = 0.0185, wR_2 = 0.0194, and GOF = 1.33, whereas the split model gave R_1 = 0.0181, wR_2 = 0.0183, and GOF = 1.26. The difference the two models had on the refined Cu−O bond lengths was very minimal, about ± 0.001 Å, and about ± 0.005 $Å^2$ on ΔU_{obs}. Therefore, for the sake of simplicity and because the split and unsplit models gave essentially the same d(Cu−O) and ΔU_{obs} values, the selenates were refined as unsplit.

(24) *teXsan*: Molecular Structure Corporation: The Woodlands, TX, 1992.

(25) Euler, H.; Barbier, B.; Meents, A.; Kirfel, A. *Z. Kristallogr.* **2009**, *351*, 351−354.

(26) Euler, H.; Barbier, B.; Meents, A.; Kirfel, A. *Z. Kristallogr.* **2003**, *218*, 265−268.
(27) (a) Shields, K. G.; Kennard, C. H. L. *Inorg. Nucl. Chem. Lett.* **1973**, *9*, 917−919. (b) Whitnall, J. M.; Kennard, C. H. L. *J. Solid. State Chem.* **1977**, *22*, 379−383.
(28) Fleck, M.; Kolitsch, U. *Z. Kristallogr.* **2002**, *217*, 15−16.
(29) δ values for the other selenate Tutton's salts are as follows: $K_2[M(H_2O)_6](SeO_4)_2$ (M = Mg, Co, Ni), 0.45, 0.44, and 0.41 Å; $Rb_2[M(H_2O)_6](SeO_4)_2$ (M = Mg, Mn, Co, Ni), 0.26, 0.28, 0.25, and 0.23 Å; and $Tl_2[M(H_2O)_6](SeO_4)_2$ (M = Mg, Mn, Co, Ni, Cu, Zn), 0.27, 0.25, 0.22, 0.22, 0.26, and 0.22 Å; see Supporting Information S1A. For the cesium salts, we define a modified δ (δ') to be the deviation of the longest of the nine X···O distances from their average. Accordingly, δ' values for $Cs_2[M(H_2O)_6](SeO_4)_2$ (M = Mg, Mn, Co, Ni, Zn) are 0.25, 0.29, 0.29, 0.29, and 0.29 Å, respectively; thus, based on these values, Cs^+ should be classified as 9-fold coordinate.
(30) (a) Bosi, F.; Belardi, G.; Ballirano, P. *Am. Mineral.* **2009**, *94*, 74−82. (b) Baur, W. H. *Inorg. Nucl. Chem. Lett.* **1972**, *8*, 1057−1061. (c) Baur, W. H. *Acta Crystallogr.* **1973**, *B29*, 139−140.
(31) (a) Baur, W. H. *Inorg. Nucl. Chem. Lett.* **1972**, *8*, 1057−1061. (b) Baur, W. H. *Acta Crystallogr.* **1973**, *B29*, 139−140. (c) Ballirano, P.; Belardi, G.; Bosi, F. *Acta Crystallogr.* **2007**, *B63*, m164−m165.
(32) δ values for the other sulfate Tutton's salts are as follows: $Na_2[M(H_2O)_6](SO_4)_2$ (M = Co), 0.23 Å; $K_2[M(H_2O)_6](SO_4)_2$ (M = Mg, Fe, Co, Ni), 0.33, 0.32, 0.31, and 0.30 Å; $Rb_2[M(H_2O)_6](SO_4)_2$ (M = Mg, Cr, Mn, Fe, Co, Ni), 0.19, 0.22, 0.18, 0.16, 0.16, and 0.17 Å; and $Tl_2[M(H_2O)_6](SO_4)_2$ (M = Mg, Mn, Fe, Co, Ni, Zn), 0.28, 0.26, 0.23, 0.24, 0.23, and 0.23 Å; Supporting Information S1B. For the cesium salts, we define a modified δ (δ') to be the deviation of the longest of the nine X···O distances from their average. Accordingly, δ' values for $Cs_2[M(H_2O)_6](SO_4)_2$ (M = Mg, Cr, Mn, Fe, Co, Ni, Cu, Zn) are 0.19, 0.30, 0.23, 0.24, 0.22, 0.23, 0.29, and 0.24 Å, respectively; thus, based on these values, Cs^+ should be classified as 9-fold coordinate.
(33) Although the X cations interact with the O(7) and O(8) waters of the $[M(H_2O)_6]^{2+}$ ion in Tutton's salts, their X···O distances are considerably more distant than the water−selenate hydrogen-bonding O−H···O distances; Table 2A and B and Supporting Information S1A and S1B. Furthermore, the differentials of the two X···O distances are nearly constant, regardless of the X cation and $[M(H_2O)_6]^{2+}$ ion; thus, these interactions do not seem to be involved in determining the form adopted by the $[M(H_2O)_6]^{2+}$ ion.
(34) Augustyniak-Jablokow, M. A. *J. Phys. Chem. Solids* **2001**, *62*, 1319−1326. A statement made in the article to the effect that EPR data show that the particular form adopted by the $[Cu(H_2O)_6]^{2+}$ ion in Tutton's salts is determined by the monovalent X cation is partly acceptable; it is true that all $[Cu(H_2O)_6]^{2+}$ ions in *sulfate* Tutton's salts adopt form **A** regardless of the alkali metal cation; however, this generalization, if intended, does not apply to the *selenate* Tutton's salts, as $[Cu(H_2O)_6]^{2+}$ in potassium-selenate adopts form **B**.
(35) Δ values for the non-JT selenate Tutton's salts are as follows: K^+ (form **B**) = 0.109(3), Rb^+ (form **A**) = 0.070(7), Tl^+ (form **A**) = 0.078(10), and Cs^+ (form **A**) = 0.045(6) Å; see Supporting Information 2A. Δ values for the non-JT sulfate Tutton's salts are as follows: Na^+ (form **A**) 0.080, K^+ (form **A**) = 0.089(4), Rb^+ (form **A**) = 0.056(6), Tl^+ (form **A**) = 0.048(3), and Cs^+ (form **A**) = 0.025(6) Å; Supporting Information S2B.
(36) Simmons, C. J.; Stratemeier, H.; Hitchman, M. A. Unpublished results.
(37) Reinen, D.; Friebel, C. *Struct. Bonding (Berlin)* **1979**, *37*, 2−60.
(38) Masters, V. M.; Riley, M. J.; Hitchman, M. A. *Inorg. Chem.* **2001**, *40*, 843−849.
(39) (a) Dobe, C.; Andres, H.-P.; Tregenna-Piggott, P. L. W.; Mossin, S.; Weihe, H.; Janssen, S. *Chem. Phys. Lett.* **2002**, *362*, 387−396. (b) Dobe, C.; Noble, C.; Carver, G.; Tregenna-Piggott, P. L. W.; McIntyre, G. J.; Barra, A.-L.; Neels, A.; Janssen, S.; Juranyi, F. *J. Am. Chem. Soc.* **2004**, *126*, 16639−16652.
(40) The Δ model's prediction for the percentage of K^+ dopant required to reach the cutoff value for the **A** → **B** transition for mixed $K_{2x}Tl_{2-2x}[Cu(H_2O)_6](SeO_4)_2$ crystals is ∼ 32% K^+ $\Delta(Tl^+)$ = 0.078 Å, as less dopant is required than for the mixed K^+/Rb^+ series because pure $Tl_2[M(H_2O)_6](SeO_4)_2$ has a smaller orthorhombic strain than $Rb_2[M(H_2O)_6](SeO_4)_2$; $\Delta(Rb^+)$ = 0.070 Å. We are currently collecting X-ray data on this series of complexes in order to substantiate the validity of the prediction.
(41) Interestingly, the situation is just the opposite for pure $Rb_2[Cu(H_2O)_6](SO_4)_2$ and $K_2[Cu(H_2O)_6](SO_4)_2$: here, the K^+ complex shows a greater temperature dependence of EPR *g* values[42] and Cu−O(7) and Cu−O(8) bond lengths[43] by virtue of its larger Δ value (orthorhombic strain is inversely proportional to Δ), $\Delta(K^+)$ = 0.089 Å and $\Delta(Rb^+)$ = 0.056 Å; both are 8-fold coordinate, and the complex with the smaller cation has less orthorhombic strain.
(42) Riley, M. J.; Hitchman, M. A.; wan Mohammed, A. *J. Chem. Phys.* **1987**, *87*, 3766−3778.
(43) Simmons, C. J.; Stratemeier, H.; Hitchman, M. A. Unpublished results.
(44) It is to be noted that the temperature dependence of the Cu−O(7) and Cu−O(8) bond lengths in $K_2[Cu(H_2O)_6](SeO_4)_2$ is much greater than in $(NH_4)_2[Cu(H_2O)_6](SeO_4)_2$, which shows very minor variations and little cooperativity from 0 to 350 K.[43,45]
(45) Kockelmann, W.; Meents, A.; Kirfel, A. *Appl. Phys* **2002**, *A74*, S1329−S1332.
(46) Figgis, B. N.; Reynolds, P. A.; Hanson, J. C.; Mutikaine, I. *Phys. Rev. B* **1993**, *48*, 13372−13377.
(47) Maaskant, W. J. A.; de Graaff, R. A. G. *J. Chem. Educ.* **1986**, *63*, 966−969.
(48) Augustyniak-Jablokow, M. A.; Yablokov, Yu. V. *Solid State Commun.* **2000**, *115*, 439−443. Yablokov, Yu. V.; Usachev, A. E.; Ivanova, T. A. *Russ. J. Coord. Chem.* **1997**, *23*, 31−44.
(49) The pressure dependence of the EPR spectra of powdered samples of Cu^{2+}-doped $K_2[Zn(H_2O)_6](SO_4)_2$ and pure $K_2[Cu(H_2O)_6](SO_4)_2$ at 300 K from 1 to 11.6 kbar showed no evidence of a switch from form **A** to **B**.[7]
(50) Bersuker, I. B. *The Jahn-Teller Effect and Vibronic Interactions in Modern Chemistry*; Plenum: New York, 1984.
(51) Bebendorf, J.; Bürgi, H.-B.; Gamp, E.; Hitchman, M. A.; Murphy, A.; Reinen, D.; Riley, M. J.; Stratemeier, H. *Inorg. Chem.* **1996**, *35*, 7419−7429.
(52) Silver, B.; Getz, D. *J. Chem. Phys.* **1974**, *61*, 638−650.
(53) (a) Petrashen, V. E.; Yablokov, Yu. V.; Davidovitch, R. L. *Phys. Status Solidi B* **1980**, *101*, 117−125. (b) Ellis, P. J.; Freeman, H.; Hitchman, M. A.; Reinen, D.; Wagner, B. *Inorg. Chem.* **1994**, *33*, 1249−1250. (c) Masters, V. M.; Riley, M. J.; Hitchman, M. A. *J. Synchrotron Rad.* **1999**, *6*, 242−243.
(54) Riley, M. J.; Hitchman, M. A.; Reinen, R. *Chem. Phys.* **1986**, *102*, 11−28.
(55) Hitchman, M. A.; Yablokov, Y. V.; Petrashen, V. E.; Augustyniak-Jablokow, M. A.; Stratemeier, H.; Riley, M. J.; Lukaszewicz, K.; Tomaszewski, P. E.; Pietrasko, A. *Inorg. Chem.* **2002**, *41*, 229−238.
(56) (a) Barashkov, M. V.; Zazhogin, A. A.; Komyak, A. I.; Shashkov, S. N. *J. Appl. Spectrosc.* **2000**, *67*, 605−611. (b) Jenkins, T. E.; Lewis, J. *Spectrochim. Acta* **1981**, *37A*, 47−50. (c) Singh, B.; Gupta, S. P.; Khanna, B. N. *Pramana* **1982**, *18*, 427−437. (d) James, D. W.; Whitnall, J. M. *J. Raman Spectrosc.* **1978**, *7*, 225−229. (e) Barashkov, M. V.; Komyak, A. I.; Shashkov, S. N. *J. Appl. Spectrosc.* **2000**, *67*, 216−224. (f) Sekar, G.; Ramakrishnan, V.; Aruldhas, G. *J. Solid State Chem.* **1988**, *74*, 424−427. (g) Choudhury, P.; Ghosh, B.; Patel, M. B.; Bist, H. D. *J. Raman Spectrosc.* **1985**, *16*, 149−155.
(57) Bill, H. In *The Dynamical Jahn-Teller Effect in Localized Systems*; Perlin,Yu. E., Wagner, M., Eds.; North Holland: Amsterdam,1984; p 791.
(58) Hitchman, M. A.; Waite, T. D. *Inorg. Chem.* **1976**, *15*, 2155−2158.
(59) Figgis, B. N.; Sobolev, A. N.; Simmons, C. J.; Hitchman, M. A.; Stratemeier, H.; Riley, M. J. *Acta Crystallogr.* **2000**, *B56*, 438−443.

(60) (a) Simmons, C. J.; Hathaway, B. J.; Amornjarusiri, K.; Santarsiero, B. D.; Clearfield, A. *J. Am. Chem. Soc.* **1987**, 1947−1958. (b) Simmons, C. J. *New J. Chem.* **1993**, *17*, 77−95.
(61) Headlam, H.; Hitchman, M. A.; Stratemeier, H.; Smits, J. M. M.; Beurskens, P. T.; de Boer, E.; Janssen, G.; Gatehouse, B. M.; Deacon, G. B.; Ward, G. N.; Riley, M. J.; Wang, D. *Inorg. Chem.* **1995**, *34*, 5516−5523.
(62) Stratemeier, H.; Wagner, B.; Krausz, E. R.; Linder, R.; Schmidtke, H.-H.; Pebler, J.; Hatfield, W. E.; ter Haar, L.; Reinen, D.; Hitchman, M. A. *Inorg. Chem.* **1994**, *33*, 2320−2329.
(63) Stebler, M.; Bürgi, H.-B. *J. Am. Chem. Soc.* **1987**, *109*, 1395−1401.